

# Spectroscopic survey of M-type asteroids<sup>1</sup>

S. Fornasier<sup>1,2</sup>, B. E. Clark<sup>3,1</sup>, E. Dotto<sup>4</sup>,  
A. Migliorini<sup>5</sup>, M. Ockert-Bell<sup>3</sup>, M.A. Barucci<sup>1</sup>

---

---

<sup>1</sup> LESIA, Observatoire de Paris, 5 Place Jules Janssen, F-92195 Meudon Principal  
Cedex, France

<sup>2</sup> Université de Paris 7 *Denis Diderot*, France

<sup>3</sup> Department of Physics, Ithaca College, Ithaca, NY 14850, USA

<sup>4</sup> INAF, Osservatorio Astronomico di Roma, via Frascati 33, I-00040 Monteporzio  
Catone (Roma), Italy

<sup>5</sup> IASF-INAF, via del Fosso del Cavaliere 100, 00133 Roma, Italy

Submitted to *Icarus*: September 2009

e-mail: [sonia.fornasier@obspm.fr](mailto:sonia.fornasier@obspm.fr); fax: +33145077144; phone: +33145077746

Manuscript pages: 60; Figures: 10; Tables: 6

---

<sup>1</sup>Based on observations carried out at the European Southern Observatory (ESO), La Silla, Chile, ESO proposals 073.C-0622, 074.C-0049 and 078.C-0115 and at the Telescopio Nazionale Galileo, Canary Islands, Spain.

**Running head:** Investigation of M-type asteroids

*Send correspondence to:*

Sonia Fornasier

LESIA-Observatoire de Paris

Batiment 17

5, Place Jules Janssen

92195 Meudon Cedex

France

e-mail: [sonia.fornasier@obspm.fr](mailto:sonia.fornasier@obspm.fr)

fax: +33145077144

phone: +33145077746

# Spectroscopic survey of M-type asteroids<sup>1</sup>

S. Fornasier<sup>1,2</sup>, B. E. Clark<sup>3,1</sup>, E. Dotto<sup>4</sup>,  
A. Migliorini<sup>5</sup>, M. Ockert-Bell<sup>3</sup>, M.A. Barucci<sup>1</sup>

---

## Abstract

M-type asteroids, as defined in the Tholen taxonomy (Tholen, 1984), are medium albedo bodies supposed to have a metallic composition and to be the progenitors both of differentiated iron-nickel meteorites and enstatite chondrites. We carried out a spectroscopic survey in the visible and near infrared wavelength range (0.4-2.5  $\mu\text{m}$ ) of 30 asteroids chosen from the population of asteroids initially classified as Tholen M-types, aiming to investigate their surface composition. The data were obtained during several observing runs during the years 2004-2007 at the TNG, NTT, and IRTF telescopes. We computed the spectral slopes in several wavelength ranges for each observed asteroid, and we searched for diagnostic spectral features. We confirm a large variety of spectral behaviors for these objects as their spectra are extended into the near-infrared, including the identification of weak absorption bands, mainly of the 0.9  $\mu\text{m}$  band tentatively attributed to orthopyroxene, and of the 0.43  $\mu\text{m}$  band that may be associated to chlorites and Mg-rich serpentines or pyroxene minerals such as pigeonite or augite. A comparison with previously published data indicates that the surfaces of several asteroids belonging to the M-class may vary significantly.

We attempt to constrain the asteroid surface compositions of our sample by looking for

---

<sup>1</sup>Based on observations carried out at the European Southern Observatory (ESO), La Silla, Chile, ESO proposals 073.C-0622, 074.C-0049 and 078.C-0115 and at the Telescopio Nazionale Galileo, Canary Islands, Spain.

meteorite spectral analogues in the RELAB database and by modelling with geographical mixtures of selected meteorites/minerals. We confirm that iron meteorites, pallasites, and enstatite chondrites are the best matches to most objects in our sample, as suggested for M-type asteroids. For 22 Kalliope, we demonstrate that a synthetic mixture obtained enriching a pallasite meteorite with small amounts (1-2%) of silicates well reproduce the spectral behaviour including the observed  $0.9 \mu\text{m}$  feature.

The presence of subtle absorption features on several asteroids confirms that not all objects defined by the Tholen M-class have a pure metallic composition.

A statistical analysis of spectral slope distribution versus orbital parameters shows that our sample originally defined as Tholen M-types tend to be dark in albedo and red in slope for increasing value of the semi-major axis. However, we note that our sample is statistically limited by our number of objects (30) and slightly varying results are found for different subsets. If confirmed, the albedo and slope trends could be due to a difference in composition of objects belonging to the outer main belt, or alternatively to a combination of surface composition, grain size and space weathering effects.

*Keywords:* Asteroids, Spectroscopy, Meteorites

---

## 1. Introduction

Within the taxonomic system of Tholen (1984), M asteroids have featureless spectra and red spectral slope over the visible wavelength range ( $0.34 - 1.04 \mu\text{m}$ ) and medium visual albedos ( $0.1 - 0.3$ ). Tholen and Barucci (1989) identify approximately 40 M-type asteroids using the Tholen (1984) class definition. The M-types are presumed to be the progenitors both of differentiated iron-nickel meteorites and enstatite chondrites (Gaffey 1976; Cloutis et al. 1990; Gaffey et al. 1993). Some authors have proposed alternative meteorite linkages, such as CH, CB (Bencubbinite) (Hardersen et al. 2005), or other carbonaceous chondrites (Vilas 1994). M-class albedos generally match those of nickel-iron meteorites, leading some to propose that these asteroids are the collisionally-produced fragments of differentiated metal cores (Bell et al. 1989). This interpretation requires parent bodies heated to at least  $2000^\circ\text{C}$  to produce iron meteorites (Taylor, 1992). However, based on recent findings, these interpretations are being challenged. Polarimetric measurements (Lupisko & Belskaya 1989) and radar observations (Ostro et al. 1991; 2000; Magri et al. 2007; Shepard et al. 2008) of selected M-type asteroids have revealed a large variety of surface properties that are in some cases inconsistent with only a metallic composition. Shepard et al. (2008), in a radar survey of 14 M-type asteroids, find that only four objects (16 Psyche, 216 Kleopatra, 758 Mancunia, and 785 Zwetana) have radar albedos high enough to be dominantly metallic.

The first estimations of the bulk density of M-asteroids 16 Psyche ( $1.4-1.8 \text{ g/cm}^3$ ) and 22 Kalliope ( $2.4 \text{ g/cm}^3$ ) gave values surprisingly lower than expected (Viateau 2000; Kocheva 2003; Britt et al. 2002; Margot & Brown 2003). These low densities are not consistent with predominantly metal composition, and require very high values for the bulk porosity. However, these values have been disputed and recently Shepard et al. (2008) estimates a very high bulk density for 16 Psyche ( $7.6 \pm 3.0 \text{ g/cm}^3$ ), more consistent with a metal composition. Descamps et al. (2008) find a bulk density of  $3.35 \pm 0.33 \text{ g/cm}^3$  for 22 Kalliope, higher than the first estimation but still implying a high bulk porosity.

Of note is the evidence for hydrated minerals on the surfaces of some M-type asteroids (Jones et al. 1990; Rivkin et al. 1995; 2000; 2002), inferred from the identification of an absorption feature around  $3 \mu\text{m}$  typically due to the first overtone of  $\text{H}_2\text{O}$  and to OH vibrational fundamentals in hydrated silicates. Rivkin et al. (1995; 2000) proposed splitting the M-types into *wet* W-class asteroids (those which show the  $3 \mu\text{m}$  band), and *dry* M-class asteroids (those which do not show the  $3 \mu\text{m}$  band). If the  $3 \mu\text{m}$  band on M-type asteroids is due to hydrated

minerals, then these objects might not be anhydrous and igneous as previously believed and the thermal scenarios for the inner main belt may need a revision (e.g. Bell et al. 1989). Gaffey et al. (2002) propose alternative explanations for the 3  $\mu\text{m}$  band: materials normally considered to be anhydrous containing structural OH; troilite, an anhydrous mineral that shows a feature at 3  $\mu\text{m}$ , or xenolithic hydrous meteorite components on asteroid surfaces from impacts and solar wind implanted H.

Recent spectroscopic observations in the visible and near infrared region show that the spectra of M asteroids are not uniformly featureless as previously believed. In addition to the 3  $\mu\text{m}$  band, faint absorption bands in the 0.9  $\mu\text{m}$  region have been identified on the surfaces of some M-type asteroids (Chapman & Gaffey, 1979; Hardersen et al. 2005; Clark et al. 2004a; Ockert-Bell et al. 2008), and attributed to orthopyroxene. Busarev (1998) detected weak features tentatively attributed to pyroxenes (0.51  $\mu\text{m}$ ) and oxidized or aqueously altered mafic silicates (0.62 and 0.7  $\mu\text{m}$ ) in the spectra of the M-type asteroids 75 Eurydike and 201 Penelope (Busarev 1998).

In this paper we present new spectroscopic data obtained in the visible and near infrared wavelength range (0.4-2.5  $\mu\text{m}$ ) of 30 asteroids sampled from the population of objects whose visible wavelength and albedo properties satisfy the definition of the Tholen M-class. In this work, we (1) identify faint absorption bands which may help reconstruct surface composition, (2) search for meteorite spectral analogues, and (3) model surface composition with geographical mixtures of selected minerals when a meteorite match is not found.

## 2. Data Acquisition

[HERE TABLE 1]

The data presented in this work were obtained during 2 runs (February and November 2004) at the Italian Telescopio Nazionale Galileo (TNG) of the European Northern Observatory (ENO) in La Palma, Spain, and 3 runs (May 2004, August 2005, and January 2007) at the New Technology Telescope (NTT) of the European Southern Observatory (ESO), in Chile. Six asteroids, investigated in the visible range at the NTT and TNG telescopes, were separately observed in the near infrared at the Mauna Kea Observatory 3.0 m NASA Infrared Telescope Facility (IRTF) in Hawaii during several runs in 2004-2008 (Table 1). Our survey was devoted to the investigation of asteroids belonging to the E, M and X classes, following the Tholen (1984) taxonomy. Here we present the results of our observations sampling within the Tholen M-class. The results from Tholen E-type

asteroids were published in Fornasier et al. (2008) and the results from Tholen X-type observations will be presented in a separate paper.

### *2.1. Observations at the TNG Telescope*

At the TNG telescope, for visible spectroscopy we used the Dolores (Device Optimized for the LOw RESolution) instrument equipped with the low resolution red grism (LR-R) covering the 0.51–0.95  $\mu\text{m}$  range with a spectral dispersion of 2.9  $\text{\AA}/\text{px}$  (see <http://www.tng.iac.es/instruments/lrs>). Most of the objects were also observed with the low resolution blue grism (LR-B, dispersion of 2.8  $\text{\AA}/\text{px}$ ) in February 2004, covering the 0.4–0.8  $\mu\text{m}$  range, and with the medium resolution blue grism (MR-B, dispersion of 1.7  $\text{\AA}/\text{px}$ , 0.4–0.7  $\mu\text{m}$  range), for the November 2004 run. The 'red' and 'blue' spectra in the visible range were separately reduced and finally combined together to obtain spectral coverage from 0.40 to 0.95  $\mu\text{m}$ . The Dolores detector is a Loral thinned and back-illuminated CCD with 2048  $\times$  2048 pixels, with a pixel size of 15  $\mu\text{m}$  and a pixel scale of 0.275 arcsec/px. Like most of the Loral CCDs, the Dolores chip is affected by moderate-to-strong fringing at red wavelengths. Despite taking as much care as possible in the data reduction process, some asteroid spectra show residual fringing that impedes identification of absorption bands in the 0.9  $\mu\text{m}$  region.

For the infrared spectroscopic investigation at the TNG telescope we used the near infrared camera and spectrometer (NICS) equipped with an Amici prism disperser. This equipment covers the 0.85–2.40  $\mu\text{m}$  range during a single exposure with a spectral resolution of about 35 (Baffa et al. 2001). The detector is a 1024  $\times$  1024 pixel Rockwell HgCdTe Hawaii array. The spectra were acquired nodding the object along the spatial direction of the slit, in order to obtain alternating pairs (named A and B) of near-simultaneous images for the background removal. For both the visible and near infrared observations we utilized a 1.5 arcsec wide slit, oriented along the parallactic angle to minimize the effect of atmospheric differential refraction.

### *2.2. Observations at the NTT Telescope*

At the NTT telescope, visible spectra were acquired using the EMMI instrument, equipped with a 2x1 mosaic of 2048 $\times$ 4096 MIT/LL CCD with square 15 $\mu\text{m}$  pixels (D'odorico, 1990). We used the grism #1 (150 gr/mm) in RILD mode to cover the wavelength range 4100–9600  $\text{\AA}$  with a dispersion of 3.1  $\text{\AA}/\text{px}$  at the first order. For the near infrared spectroscopy, we utilized the instrument SOFI (Son OF Isaac) in the low resolution mode. The blue and red grisms, covering respectively the 0.95–1.64  $\mu\text{m}$  (dispersion of 6.96  $\text{\AA}/\text{px}$ ) and the 1.53–2.52  $\mu\text{m}$  range

(dispersion of  $10.22 \text{ \AA}/\text{px}$ ) were used (Moorwood et al., 1998). The acquisition technique was identical to that used for the TNG observations, however we used a larger slit (2 arcsec), always oriented along the parallactic angle. The two spectral regions of the blue and red grism observations were combined matching the overlapping region in the  $1.53\text{--}1.64 \mu\text{m}$  range.

### 2.3. Observations at the IRTF Telescope

At the IRTF telescope we used the SpeX instrument, equipped with a cooled grating and an InSb array ( $1024 \times 1024$ ) spectrograph at wavelengths from  $0.82$  to  $2.49 \mu\text{m}$ . (Rayner et al. 2003). Spectra were recorded with a slit oriented in the north-south direction and opened to  $0.8$  by  $15$  arcseconds. A dichroic lens reducing the signal below  $0.8 \mu\text{m}$  was used for all observations. Objects were consistently observed near the meridian to minimize airmass, but total integration time varied from  $\sim 6$  to  $30$  minutes, depending on the strength of the signal relative to sky lines.

## 3. Data Reduction

Visible and near-infrared spectra were reduced using ordinary procedures of data reduction with the software packages Midas and IDL as described in Fornasier et al. (2004a,b). For the visible spectra, the procedure includes the subtraction of the bias from the raw data, flat-field correction, cosmic ray removal, sky subtraction, collapsing the two-dimensional spectra to one dimension, wavelength calibration, and atmospheric extinction correction. The reflectivity of each asteroid was obtained by dividing its spectrum by that of the solar analog star closest in time and airmass to the object. Spectra were finally smoothed with a median filter technique, using a box of  $19$  pixels in the spectral direction for each point of the spectrum. The threshold was set to  $0.1$ , meaning that the original value was replaced by the median value if the median value differs by more than  $10\%$  from the original one.

For observations in the infrared range, spectra were first corrected for flat fielding, then bias and sky subtraction was performed by producing A-B and B-A frames. The positive spectrum of the B-A frame was shifted and added to the positive spectrum of the A-B frame. The final spectrum is the result of the mean of all pairs of frames previously combined. The spectrum was extracted and wavelength calibrated. For the NTT-SOFI spectra, this last step was performed acquiring the spectrum in the blue and red grisms of a Xenon lamp, and comparing the observed lines with those of a reference table, obtaining the dispersion relation. For

the TNG-NICS spectra, due to the very low resolution of the Amici prism, the lines of Ar/Xe lamps are blended and cannot be easily used for standard reduction procedures. For this reason, the wavelength calibration was obtained using a look-up table which is based on the theoretical dispersion predicted by ray-tracing and adjusted to best fit the observed spectra of calibration sources. Finally, the extinction correction and solar removal was obtained by division of each asteroid spectrum by that of the solar analog star closest in time and airmass to the object. For the IRTF data, after the normal data reduction procedures of flat-fielding, sky subtraction, spectrum extraction, and wavelength calibration, each spectrum was fitted with the ATRAN atmospheric model for telluric absorption features (Lord 1992; Bus et al. 2002a, 2003; Sunshine et al. 2004). This procedure required an initial estimate of precipitable water in the atmospheric optical path using the zenith angle for the observation and the known  $\tau$ -values (average atmospheric water) for Mauna Kea. This initial guess was iterated until the best fit between predicted and observed telluric band shapes was obtained, and an atmospheric model spectrum was generated (Bus et al. 2003). Following this, each asteroid spectrum was divided by the atmospheric model and then ratioed to each star spectrum, similarly reduced, before normalization at  $1.2 \mu\text{m}$ . The software and procedures used for data reduction are described in DeMeo et al. (2009). The final spectra we report are averages of 3-5 asteroid/star ratios, calculated to minimize variations due to standard star and sky variability. Usually, 2-5 different standard stars were observed on any given night at the telescope. We used only solar standard stars, and each standard star was observed 1-3 times per night.

The stellar and asteroid spectra were cross-correlated and, if necessary, sub-pixel shifts were made before ratioing the asteroid to the star. This reduction step is needed to reduce the noise and/or the changes in the final asteroid slope due to small changes in the wavelength dispersion between asteroid and star observations, introduced by instrumental flexure.

The infrared and visible spectral ranges of each asteroid were finally combined by overlapping the spectra, merging the two wavelength regions at the common wavelengths and utilizing the zone of good atmospheric transmission to find the normalization factor between the two spectral parts. For the TNG and IRTF data the overlapping region goes from  $\sim 0.86$  to  $0.94 \mu\text{m}$ , and we took the average value over the  $0.89$ - $0.91 \mu\text{m}$  region of the visible spectrum to normalize the infrared spectrum. For the NTT data, the overlapping region is very small so we took the average value over the  $0.95$ - $0.96 \mu\text{m}$  region to normalize the spectra. The spectra of the observed asteroids, all normalized at  $0.55 \mu\text{m}$ , are shown in Figures 1–5. Observational conditions are reported in Table 1.

[Here Figs 1, 2, 3, 4, 5]

#### 4. Results: Spectral Analysis and Absorption Features

[HERE TABLE 2 and 3]

We present new spectra of 30 asteroids whose visible wavelength properties and albedos fall within the boundaries of the M-class as defined by Tholen (1984). We obtained new visible spectra for 6 objects, and new visible and near-infrared spectra for 24 objects (Figures 1–5).

To analyze the data, spectral slope values were calculated by a linear fit to different wavelength regions:  $S_{cont}$  is the spectral slope in the whole range (continuum slope) observed for each asteroid,  $S_{VIS}$  is the slope in the 0.55-0.80  $\mu\text{m}$  range,  $S_{NIR1}$  is the slope in the 1.1-1.6  $\mu\text{m}$  range, and  $S_{NIR2}$  is the slope in the 1.7-2.4  $\mu\text{m}$  range. Values are reported in Table 2, together with the asteroid’s physical and orbital parameters, and the Bus-DeMeo classifications (Bus & Binzel 2002b; DeMeo et al. 2009) derived respectively from the visible and VIS-NIR spectrum. Band centers and depths were calculated for each asteroid showing an absorption feature, following the Gaffey et al. (1993) method. First, a linear continuum was fitted at the edges of the band, that is at the points on the spectrum outside the absorption band being characterized. Then the asteroid spectrum was divided by the linear continuum and the region of the band was fitted with a polynomial of order 2 or more. The band center was then calculated as the position where the minimum of the spectral reflectance curve occurs, and the band depth as the minimum in the ratio of the spectral reflectance curve to the fitted continuum (see Table 3).

The infrared data reveal the silicatic nature of 516 Amherstia. Its spectrum exhibits the  $\sim 1$  and 2  $\mu\text{m}$  bands typically associated with olivine and pyroxene (Table 3). On this basis, we re-classify 516 as an S-type (it belongs to the Sq class in the Bus-DeMeo classification). For this reason, 516 will not be included in the following discussion. The asteroids in our sample show different spectral behaviors (Figs 1–5). Sixteen of them have spectra with at least one absorption feature (Table 3). The main feature identified is in the 0.9  $\mu\text{m}$  region, as already reported by several authors (Clark et al. 2004a; Hardersen et al. 2005; 2006a,b; 2007a,b; Ockert-Bell et al. 2008), and it is attributed to low-Fe, low-Ca orthopyroxene minerals. The band center ranges from 0.86  $\mu\text{m}$  (417 SUEVIA) to 0.97  $\mu\text{m}$  (216 KLEOPATRA), with a band depth of 1–5 % as compared to the continuum.

Some asteroids (16 Psyche, 22 Kalliope, 69 Hesperia, 216 Kleopatra, 338 Budoza, and 498 Tokio) show an additional faint feature at  $\sim 0.43 \mu\text{m}$  (Table 3). This band is not easily attributable: it might be associated with chlorites and Mg-rich

serpentines as suggested by King & Clark (1989) for enstatite chondrites; with pyroxene minerals such as pigeonite or augite as suggested by Busarev (1998) for M-asteroids; or to an  $\text{Fe}^{3+}$  spin-forbidden transition in the iron sulfate jarosite, as suggested by Vilas et al. (1993) for low-albedo asteroids. Within our sample, Rivkin et al. (1995; 2000) detected the  $3 \mu\text{m}$  absorption band on 22 Kalliope, 55 Pandora, 110 Lydia, 129 Antigone, 135 Hertha, 201 Penelope (they proposed the *W wet* class for these bodies), and they suggested that this feature can be attributed to the presence of hydrated phases on their surfaces (Table 3). We detect the  $0.43 \mu\text{m}$  band only on one W asteroid (22 Kalliope). If this feature is actually due to the presence of chlorites–Mg rich serpentines and/or to jarosite, this might support the interpretation of the  $3 \mu\text{m}$  band as due to aqueous alteration products. The other W asteroids do not show the  $0.43 \mu\text{m}$  feature, while it *is* present in the spectra of two asteroids not having the  $3 \mu\text{m}$  absorption (16 Psyche and 216 Kleopatra). We conclude that there is no correlation between the  $0.43$  and  $3 \mu\text{m}$  bands.

Asteroid 132 Aethra shows a faint band centered at  $\sim 0.49 \mu\text{m}$  that resembles the absorption seen on some E-type (subclass EII) asteroids (Fornasier et al. 2007; 2008; Clark et al. 2004b), where it is attributed to sulfides such as oldhamite and/or troilite (Burbine et al. 1998; 2002a; 2002b). We obtained only one spectrum in the visible range and no other observations are available in the near infrared nor in the  $3 \mu\text{m}$  region. Bus and Binzel (2002b) gave 132 Aethra an Xe designation, and its IRAS albedo is 0.2 (Table 4).

Asteroid 135 Hertha has a faint band at  $\sim 0.51 \mu\text{m}$ , narrower than that seen on EII asteroids or Aethra, and similar to the  $\text{Fe}^{2+}$  spin-forbidden crystal field transitions in Earth and lunar pyroxene (Burns et al. 1973, Adams 1975, Hazen et al. 1978). This band has been previously detected by Busarev (1998) on the surface of two other M asteroids, 75 Eurydike and 201 Penelope (however our visible spectrum of 201 does not show any feature detectable within the noise of the data).

125 Liberatrix was observed 3 times on November 20, 2004. The three spectra are shown in Fig. 1, and were obtained  $\sim 1.5$  hours apart, covering  $\sim 75\%$  of the Liberatrix rotational phase (period of 3.97 hours). The spectra are very similar (Fig. 1) so, in this region of the rotational phase, the body appears to have a homogeneous surface composition. There is a hint of an absorption band in the  $0.9 \mu\text{m}$  region, also seen by Hardersen et al. (2005), however we cannot clearly identify it due to the aforementioned fringing in this region. The features at  $0.48$  and  $0.52 \mu\text{m}$  are spurious residuals of the flat field.

#### 4.1. Comparison with Existing Literature Data

Hardersen et al. (2005) report the presence of absorption bands in the  $0.9 \mu\text{m}$  region on 16 Psyche, 69 Hesperia, 110 Lydia and 216 Kleopatra (and an absence of absorption features on 325 Heidelberga, within the scatter of their data). Our spectra confirm the presence of an absorption feature in the  $0.9 \mu\text{m}$  region, but our band center values are higher than those reported by Hardersen et al. (2005). They found the band also on 125 Liberatrix and 201 Penelope, which we observed only in the visible region with the TNG telescope, and which show an indication of a faint absorption feature (Fig 1). Nevertheless, due to the fringing problems and low sensitivity of the detector in this wavelength region, we cannot clearly confirm that an absorption band is present, nor can we quantify it. The difference in the band center location might be due to different methodologies in data analysis (choice of continuum removal or imperfect removal of the telluric water vapor feature), but we cannot exclude that it is real and associated with variations in the orthopyroxene content over the asteroid's surface.

Birlan et al. (2007) observed 9 M-type asteroids, and they did not report the presence of absorption features. Three of their objects belong also to our survey. Our spectra of 325 Heidelberga and 860 Ursina seem in agreement with the data of Birlan et al. (2007), while for 558 Carmen we obtained only a spectrum in the visible range. 558 Carmen was observed also by Hardersen et al. (2006a) through about  $1/3^{\text{rd}}$  of a full rotation, and their spectra exhibit a weak  $0.9 \mu\text{m}$  band, attributed to low-Fe pyroxenes, with band centers ranging from  $0.91$  to  $0.94 \mu\text{m}$ . The Birlan et al. (2007) spectrum is featureless, and our visible spectrum ends at  $0.91 \mu\text{m}$  so it can not help with band identification (the faint absorption around  $0.83 \mu\text{m}$  is due to incomplete removal of telluric bands). It is possible that asteroid 558 Carmen has an inhomogeneous surface composition.

325 Heidelberga was observed also by Takir et al. (2008) who found in its spectrum a weak (1-2% depth) feature center at  $0.9 \mu\text{m}$ , while our spectrum, that of Birlan et al. (2007), and of Hardersen et al. (2005) are featureless. This asteroid may have a heterogeneous surface composition and further high S/N ratio observations covering the whole rotational period are needed for a full investigation.

Hardersen et al. (2006a) detected the  $\sim 0.9 \mu\text{m}$  absorption feature also on 216 Kleopatra (center at  $0.91 \mu\text{m}$ , depth 3%), and on 347 Pariana (center varying from  $0.88$ – $0.93 \mu\text{m}$  with depth 3%, in spectra obtained through more than one asteroid full rotation). We confirm the detection of the band on these two asteroids (Table 3) with similar band parameters. Our data agree with the Hardersen et al. (2006a) finding also for 97 Klotho (featureless spectra in both case, and also for

the Klotho data presented in Ockert-Bell et al. 2008), but disagree for 498 Tokio and 129 Antigone. In fact, for 498 Tokio, Hardersen et al. (2006a) reported a blue featureless spectrum, while our data show an increasing slope up to  $\sim 0.7 \mu\text{m}$ , and then a flat spectral behavior in the near-infrared, with two faint absorption bands centered at 0.43, and  $1.16 \mu\text{m}$ . On the other hand, for 129 Antigone Hardersen et al. (2006a) found absorption features at 0.76, 0.9, 1.07, and  $1.39 \mu\text{m}$ , attributed to the presence of antigorite, which has absorption bands consistent with those of the asteroid. Our spectrum has a poor S/N ratio in the near-infrared range. We do not see the 0.76 or  $0.9 \mu\text{m}$  bands, but a broad feature in the  $0.93\text{--}1.14 \mu\text{m}$  region. The spectrum is peculiar: it has a convex shape below  $0.9 \mu\text{m}$ , then it is almost flat up to  $\sim 1.8 \mu\text{m}$  with a steep increase of the spectral slope in the  $1.8\text{--}2.0 \mu\text{m}$  region. Ockert-Bell et al. (2008) observed Antigone at different aspects, and they found the  $0.9 \mu\text{m}$  band and spectral variations in continuum slope above 20% for different rotational aspects. It is thus possible that this asteroid has an inhomogeneous surface composition.

Hardersen et al. (2007a; 2007b; 2006b) observed several asteroids reported in this survey (135 Hertha, 224 Oceana, 250 Bettina, 369 Aeria, 516 Amherstia, and 872 Holda). For 250 Bettina, our spectrum is steeper in the infrared compared to their data, but both spectra show a band in the  $0.9 \mu\text{m}$  region. For 369 Aeria, Hardersen et al. found absorption bands at 0.9 and  $1.9 \mu\text{m}$ , while our spectrum shows only the  $0.9 \mu\text{m}$  feature and a reddish spectral behavior in the NIR with a steeper spectral slope than Hardersen et al. (2007a). 224 Oceana shows similar featureless spectra and 135 Hertha has an absorption at  $0.9 \mu\text{m}$  in both surveys. 516 Amherstia shows similar  $\sim 1$  and  $2 \mu\text{m}$  features, but they are deeper in our spectrum compared to Hardersen et al (2006b). 872 Holda shows a broad and weak feature in both surveys centered at  $\sim 0.96 \mu\text{m}$ . Hardersen et al. (2006b) found that Holda is spectrally similar to synthetic troilite (Cloutis and Burbine 1999), and proposed for the surface composition of this asteroid a mixture of NiFe metal and troilite.

Four M-types (16 Psyche, 110 Lydia, 216 Kleopatra, and 785 Zwetana) of the Clark et al. (2004a) survey of the X complex were re-studied in this work. The spectral behavior of 110 Lydia and 216 Kleopatra looks quite similar, while for 16 Psyche our data show a linear NIR spectrum with an higher spectral gradient than that reported in Clark et al. (2004a), and for 785 Zwetana our NIR spectrum is almost linear and featureless, while Clark et al. (2004a) reported a convex shape spectrum and detected a feature at  $\sim 0.9 \mu\text{m}$ . Psyche was observed also by Binzel et al. (1995) over its rotation, and they did not find any significant variation in its visible reflectance spectrum within their measurement precision of 1%.

Zwetana was observed also by Hardersen et al. (2007a), who detected in its spectrum a broad and faint absorption beyond  $1.3 \mu\text{m}$ , but no features in the  $0.9\text{-}1.0 \mu\text{m}$  region, and by Ockert-Bell et al. (2008), who presented a featureless spectrum with no significant slope variations at different aspects.

755 Quintilla shows a very peculiar spectrum with several absorption bands (Fig 5, Table 3). The bands at  $0.9$  and  $1.86 \mu\text{m}$  can be attributed to orthopyroxene, however the peculiar features at  $1.37$  and  $1.61 \mu\text{m}$  are not easily interpreted. It is worth noting that Fieber-Beyer et al. (2006) find three absorption features in a Quintilla spectrum but at different central wavelengths. They interpreted bands at  $0.93$ , and  $1.7 \mu\text{m}$  as due to spinel, while the nature of the  $1.59 \mu\text{m}$  band was unknown.

In sum, comparing our spectra with those in the existing literature, we suggest that asteroids 129 Antigone, 325 Heidelberga, 498 Tokio, and 785 Zwetana may display surface variability as they show different spectral behaviors throughout independent observations. Some differences in the spectral slope values or band center positions are seen also for asteroids 16 Psyche, 250 Bettina, 369 Aeria, 516 Amherstia, 558 Carmen, and 755 Quintilla, but we cannot clearly state if they are due to real variation or simply to observational uncertainty and/or differences in data acquisition and reduction. Additional high S/N ratio observations are needed to investigate possible surface inhomogeneities for these asteroids.

## 5. From the Tholen to the Bus-DeMeo taxonomy

[HERE TABLE 4]

Our targets were classified as belonging to the Tholen M class on the basis of their spectra from  $0.4$  to  $1 \mu\text{m}$  and their moderate albedo values. Our new spectral observations enrich the available physical information for these objects and allow us to apply the Bus-DeMeo classification recently published (DeMeo et al., 2009). The Bus-DeMeo system is based on the asteroid's spectral characteristics over the wavelength range  $0.45$  to  $2.45 \mu\text{m}$  without taking the albedo into consideration. Indeed, the observed Tholen M-type asteroids show different spectral behaviors in the near infrared range. We therefore re-classified our 24 targets observed in the V+NIR range according to the Bus-DeMeo taxonomy and the corresponding classes are summarized in Table 2.

Thirteen of the 24 Tholen M-type asteroids we investigated are Xk-types in the Bus-DeMeo taxonomy. Asteroids belonging to this class have spectra characterized by a shallow absorption feature that appears as a concavity over the range  $0.8$  to  $1.0 \mu\text{m}$ , in what is otherwise a generally linear spectrum. Indeed, all 13

asteroids classified as Xk (Table 2) show a band in the 0.9  $\mu\text{m}$  region (Table 3) attributed to low-Fe, low-Ca orthopyroxene minerals. Their albedo value varies between 0.12 and 0.21, except for 2 asteroids, where it is higher (250 Bettina has an albedo of 0.25 and 55 Pandora of 0.30). Some of the Xk asteroids investigated show additional features as summarized in Table 4. A 0.43  $\mu\text{m}$  band is seen in the Xk asteroids 16, 22, 69, 216, and 338. Considering the asteroids' moderate albedo values, this band might be due to chlorites and Mg-rich serpentines or pigeonite or augite minerals.

For 755 Quintilla, the classification as Xk type seems to be questionable since Quintilla presents other features at 1.37, 1.61, and 1.87  $\mu\text{m}$ , as previously mentioned (Table 4). Finally, 135 Hertha also shows a faint feature at 0.51  $\mu\text{m}$  probably due to  $\text{Fe}^{2+}$  spin-forbidden crystal field transitions in pyroxene.

Five of the observed asteroids (Table 2) have a slightly reddish spectrum, featureless in the 0.45-2.4  $\mu\text{m}$  range, and belong to the Xc-type in the Bus-DeMeo taxonomy. Among them only 498 Tokio has a low albedo value compatible with carbonaceous chondrite analogs. It is the only Xc type that also show a feature at 0.43  $\mu\text{m}$ , that we interpret as due to the iron sulfate jarosite, and a broad absorption in the 1-1.3  $\mu\text{m}$  region usually seen in C-type asteroids (Table 4). The Xc type 129 Antigone has a band centered at 1.03  $\mu\text{m}$  possibly due to the phyllosilicate antigorite, as suggested by Hardersen et al. (2006a).

The four asteroids 325, 441, 785, and 860 have featureless spectra and follow the X class. Their albedo values vary between 0.11-0.16.

According to these new near infrared observations 516 Amherstia must be reclassified as an S-type in the Tholen classification and an Sq-type in the Bus-DeMeo system. The asteroid 849 Ara has a steep spectral slope and falls in the D class according to the Bus-DeMeo taxonomy (Table 2), but its albedo is very high (0.27), excluding a surface composition of organic-rich silicates, carbon, and anhydrous silicates as commonly expected on low-albedo Tholen D type asteroids.

## 6. Meteorite Spectral Matches

### 6.1. Methodology

To constrain the possible mineralogies of our asteroids (those with both visible and near infrared spectra), we conducted a search for meteorite and/or mineral spectral analogs. We used the publicly available RELAB spectrum library (Pieters 1983), which consisted of nearly 15,000 spectra in November of 2008. For each spectrum in the library, a filter was applied to find relevant wavelengths (0.4 to 2.45  $\mu\text{m}$ ). Then, a second filter was applied to reject spectra with irrelevant albedo

values (i.e. brightness at  $0.55 \mu\text{m}$  too high or too low). This process produced a list of approximately 4000 RELAB spectra of appropriate brightness and wavelength coverage for comparison to the asteroid. RELAB spectra were normalized to 1.0 at  $0.55 \mu\text{m}$ , and then a Chi-squared value was calculated relative to the normalized input asteroid spectrum. We used the asteroid wavelength sampling to resample the laboratory spectra by linear interpolation. This allowed a least-squares calculation with the number of points equal to the wavelength sampling of the asteroid spectrum. The RELAB data files were sorted according to Chi-squared, and then visually examined for dynamic weighting of spectral features by the spectroscopist. Given similar Chi-squared values, a match that mimicked spectral features was preferred over a match that did not. We visually examined the top 50 Chi-squared matches for each asteroid. No specific grain-size sampling filter was applied, and many of the best matches found were of slab or sanded slab (or rough-cut) surfaces.

The importance of our second filter is that we constrained the search for analogs to those laboratory spectra with brightness (reflectance at  $0.55 \mu\text{m}$ ) roughly comparable to the albedo of the asteroid. For the asteroid albedo value, we generally used the IRAS albedo published by Tedesco et al. (2002). For the darker asteroids (below 10% albedo), this is a fairly well-known number. The uncertainty for brighter asteroid albedos (above 10% albedo) is relatively larger. This is because at equivalent geocentric and heliocentric distances, a darker asteroid will have stronger thermal flux, allowing a more precise and more accurate albedo determination. To account for this, we filtered out lab spectra if brightness differed by more than  $\pm 3\%$  in absolute albedo for the darker asteroids in our sample (albedo less than 10%), and we filtered out lab spectra if brightness differed by more than  $\pm 5\%$  in absolute albedo for the brighter asteroids (albedos greater than 10%). For example, if an asteroid's albedo was 20%, we searched over all lab spectra with  $0.55 \mu\text{m}$  reflectance between 15% and 25%. If an asteroid's albedo was 7%, we searched over all lab spectra with reflectance between 4% and 10%. Once the brightness filter was applied, all materials were normalized before comparison by least-squares. We note that mismatches between asteroid albedo and meteorite  $0.55 \mu\text{m}$  reflectance occurs for a few well-known meteorite-asteroid pairings, such as Vesta (albedo about 40%) and HEDs (many of which have  $0.55 \mu\text{m}$  reflectances of 25-30%). The last filter to be applied was a "no lunar sample" filter, and this will be explained further in the next section. Our search techniques effectively emphasized the spectral characteristics of brightness and shape, and de-emphasized minor absorption bands and other parametric characteristics.

## 6.2. Meteorite Analogs

[HERE TABLE 5]

[HERE FIGURES 6, 7 and 8]

The best matches between our observed sample and meteorites (from the RELAB database) are reported in Table 5 and in Figs 6, 7, and 8. Most best matches resulted in iron meteorites (IM), pallasites (Pall), or enstatite chondrites (EC), as suggested in the literature for the M-type asteroids. Some meteorite matches are quite good, while for some asteroids (16 Psyche, 22 Kalliope, 69 Hesperia, 216 Kleopatra 755 Quintilla, 872 Holda) the best meteorite match we found does not satisfactorily reproduce both the visual and near infrared spectral behavior. The RELAB spectral library does not contain CB meteorite spectra, so the suggested analogue of CB Bencubbinites (Hardersen et al. 2005) remains spectrally untested. In contrast, the RELAB spectral library contains many samples of other carbonaceous chondrites, only one of which was found as a best match in this study (498 Tokio was best fit with a CV carbonaceous chondrite, but its albedo is anomalously low (7%) within the M class). This would seem to provide evidence against the suggestion of Vilas (1994) that carbonaceous chondrites are analogues for the M-type asteroids. In fact, CV chondrites are usually associated with K-type asteroids (Mothé-Diniz et al. 2008; Clark et al. 2009), or with B-type asteroids (Clark et al. 2010).

The only asteroid to result in an enstatite chondrite best match is 161 Athor. Neither the asteroid nor the enstatite chondrites (in general) show absorption features, so the match is purely based on spectral slope and albedo.

Iron meteorites matched both featureless asteroids (69 Hesperia, 97 Klotho, 224 Oceana, 325 Heidelberg, 849 Ara) and asteroids with bands (16 Psyche, 216 Kleopatra, 110 Lydia, 135 Hertha, 338 Budrosa, 347 Pariana, 369 Aeria, 860 Ursina, and 872 Holda). In particular, we note that RELAB file c1mb46 (of the iron meteorite Landes which has silicate inclusions) was selected as a best fit for 5 different asteroids (135 Hertha, 224 Oceana, 347 Pariana, 22 Kalliope, and 872 Holda). This spectrum shows a faint absorption band at  $0.9 \mu\text{m}$ , probably due to the silicate inclusions. Of concern, of course, is the fact that this sample was measured as a slab, not as a particulate.

Pallasites were the best matches for 785 Zwetana (no bands), 110 Lydia, 250 Bettina, 22 Kalliope, and 55 Pandora (all with bands). Several asteroid matches resulted in different RELAB spectral files (c1mb43, ckmb43, and cmmb43) of the same meteorite, the stony-iron pallasite Esquel. The differences between these spectra are that c1mb43 is of a sanded metal area on an Esquel slab, measured

from one incidence angle, while cmmb43 is of the same sanded area measured from two different incidence angle directions (averaged), and ckmb43 is a metal-rich powder of the meteorite with a grain size less than  $63 \mu\text{m}$ . In a recent paper, Cloutis et al. (2010) study in detail the physical reasons for the spectral differences observed as a function of sample preparation. This example illustrates a typical issue with a library database search. The same sample can look spectrally different depending on measurement illumination and grain size circumstances. Such spectral differences result not from compositional differences, but from measurement circumstances. This indicates that the spectral differences between the asteroids found to match these meteorites (110 Lydia, 22 Kalliope, and 55 Pandora), are insignificant according to the spectral library.

We note that the peculiar object 516 Amherstia (which we have suggested be reclassified as an S-type) was found to be similar to a laser-irradiated ordinary chondrite (OC). Similarly, asteroid 441 Bathilde was best fit with a laser-irradiated sample of olivine. Unlike 516 Amherstia, 441 Bathilde does not show absorption features, so the spectral match is based on slopes, shape, and brightness only. Nevertheless, we note with amusement that highly space weathered materials cannot be ruled out as a surface composition for 441 Bathilde, based on the excellent agreement between the asteroid and the laboratory spectra of a simulated weathered olivine.

M-type asteroid spectra, being largely featureless, were very often fit with a lunar soil sample during the automated part of our RELAB search. For example, 55 Pandora, which has a band at  $0.9 \mu\text{m}$ , was well fit with RELAB file cs65, which is a spectrum of Apollo program sample 61221,114, a lunar highland soil from the Apollo 16 landing site. Like M-type asteroids, lunar soils tend to be very steeply spectrally sloped. When they are most mature (highly space-weathered), lunar soils tend to show only very minor silicate absorption features, like M-type asteroids. Thus, without applying a "no lunar sample" filter in our search, we would have been led to the conclusion that some M-type asteroids are covered with lunar-soil-like materials.

In sum, our method of searching for meteorite analogues emphasized the spectral characteristics of brightness and shape, and de-emphasized minor absorption bands. Automated Chi-squared algorithms will always result in such an emphasis. We attempted to account for this by selecting fits with good band mimickry over poor band mimickry when Chi-squared values were comparable, however there are some cases where weak (1-2%) bands are not faithfully matched (e.g. 110 Lydia). Only spacecraft mission sample returns will ultimately allow us to answer the question "Could a 'featureless' iron meteorite be considered an analogue of

an asteroid which has a band?”

### 6.3. Statistics

[HERE TABLE 6]

[HERE FIGURE 9]

We ran a Spearman Rank Correlation (Spearman 1904) to search for possible correlations between our sample’s spectral characteristics and their orbital and physical parameters. The Spearman correlation function gives a two-element vector containing the rank correlation coefficient ( $\rho$ ) and the two-sided significance of its deviation from zero ( $P_r$ ). The value of  $\rho$  varies between -1 and 1; if  $|\rho|$  is close to zero, then there is no correlation and if  $|\rho|$  is close to 1, then a correlation exists. The significance ( $P_r$ ) is a value in the interval  $0 < P_r < 1$ . A small value indicates a significant correlation. We consider a strong correlation to have  $P_r < 0.01$  and  $|\rho| > 0.6$ , and a weak correlation to have  $P_r < 0.08$  and  $0.3 < |\rho| < 0.6$ .

Our sample includes 29 asteroids observed in the visible range. We eliminated 516 Amherstia from all further analysis because spectral properties diverge completely from all others. In fact, it displays strong 0.9 and 1.9  $\mu\text{m}$  features, putting it into the Sq-class in the Bus-DeMeo system. 23 asteroids were observed both in the visible and near infrared range. We analyse the whole sample as well as the subsamples we consider most likely to be the most metal rich (those without the 0.9  $\mu\text{m}$  absorption band) and those containing silicates, presenting the 0.9  $\mu\text{m}$  band, and belonging to the Xk type in the Bus-DeMeo taxonomy.

Among our Spearman Rank Correlation test results, we find weak anti-correlations between the slopes  $S_{cont}$ ,  $S_{NIR1}$ , and  $S_{NIR2}$ , and the asteroids’ rotational period (Table 6). Belskaya & Lagerkvist (1996) found that M-asteroids have a faster mean rotational period compared to S and C type asteroids. They interpreted this as an indication of an higher mean density that allows M-asteroids to survive energetic collisions without disruption, which increases their rotational angular momentum. One possible explanation is that fast rotators have a higher density, so they have a composition metal rich, which is characterized by steeper spectral slope. The slow M-type rotators may have a smaller mean density and so a smaller amount of metals in their composition, which is characterized by a less steep spectral slope.

From our Spearman Rank Correlation tests, there also appear to be significant correlations between slope and semi-major axis, and albedo (Table 6). The continuum slope ( $S_{cont}$ ) and the 1.1-1.6  $\mu\text{m}$  slope ( $S_{NIR1}$ ) are correlated with semi-major axis  $a$ , while the slope in the visible range ( $S_{VIS}$ ) is only weakly correlated with  $a$  (Fig. 9). Asteroids in our sample with the 0.9  $\mu\text{m}$  feature show a correlation

between  $S_{cont}$  versus  $a$ , and a weaker correlation between  $S_{NIR1}$  versus  $a$ . It must be noted that our sample size is small.

Considering all 29 asteroids in our sample, a weak anti-correlation exists between the  $S_{VIS}$  and the albedo, in particular the anti-correlation becomes stronger for asteroids not showing the silicatic band at  $0.9 \mu\text{m}$ . So the visual slope tends to increase with decreasing albedo.

The correlation of the continuum slope to the semi-major axis together with the anti correlation of the visible slope to albedo indicates that our sample derived from Tholen M-type asteroids tend to be dark in albedo and red in near-infrared slope with increasing semi-major axis. This is true in particular for 'featureless' subset of our sample that we consider most likely to be iron rich. Darkening of albedo plus reddening of the slope is a typical effect of space weathering seen on lunar samples and silicate rich asteroids. Using statistical arguments, Lazzarin et al. (2006) have shown that space weathering probably occurs on all asteroid types. Nevertheless, space weathering effects have not been fully investigated for metallic rich surfaces. If space weathering acts on M-type asteroids as it does with S type asteroids, then asteroids that are closer to the Sun might be expected to show stronger spectral changes because of the higher abundance of solar wind ions. Our results indicate an opposite trend. A few measurements exist on the effect of space weathering on enstatite chondrite and iron and stony iron meteorites (e.g. Vernazza et al. 2009). An irradiated sample of the Eagle enstatite chondrite meteorite revealed a slight reddening of the spectral slope and no more than 3% darkening of the visual albedo. For the Vaca Muerta mesosiderite meteorite Vernazza et al. (2009) found again a reddening in the spectral slope and a darkening of the visual albedo. Grain size effects can play an important role in the slope changes as well. Britt and Pieters (1988) studied the bidirectional reflectance properties of some iron-nickel meteorites for different surface roughness. They found that the spectra of M-type asteroids show good agreement with those of iron meteorites with surface features in the range of  $10 \mu\text{m}$  to  $1 \text{mm}$ , that is larger than the wavelength of incident light. Meteorites with these roughness values are diffuse reflectors and show the classic red slope continuum of iron, with practically no geometric dependence on reflection. On the other hand, a decreasing of the meteorite surface roughness changes the reflectance characteristics: complex scattering behaviour is seen for roughness in the  $0.7\text{-}10 \mu\text{m}$  range, while for roughness values  $< 0.7 \mu\text{m}$  the reflectance is characterised by two distinct components, the specular one which is bright and red sloped, and the nonspecular one which is dark and flat. Moreover, Cloutis et al. (1990) found that the spectra of three iron meteorites reddened with increasing grain size.

Thus, the correlation of the continuum slope to the semimajor axis together with the anti correlation of near-infrared slope to albedo are not easily interpreted. They may reflect a different surface composition of different M-type asteroids, and/or a combination of surface composition, grain size and space weathering effects that are not yet fully understood.

## 7. Discussion

There are 30 asteroids having M-type visible wavelength and albedo properties that were investigated in this study. One was removed due to its similarity to an S-type asteroid (516 Amherstia). Of the remaining 29 asteroids, 16 have detectable faint absorption features. The shape and slopes in the continuum, visible, and near infrared varies greatly when Tholen M-class objects have their spectral measurements extended. All were found to be classifiable in the extended wavelength taxonomy defined by DeMeo et al. (2009). Our search for meteorite analogs concluded that the shape of the spectra could be modeled by a variety of iron and stony iron meteorites, as well as pallasites, enstatite chondrites, and irradiated mixtures. However, this method of search de-emphasizes the small absorption features. To investigate the significance of the shallow absorption features found in our sample, we used a linear (geographical) spectral mixing model.

One possible avenue for investigation is the mixture of the totally featureless, red-sloped metallic meteorites with orthopyroxenes, which are thought to create the weak  $0.9 \mu\text{m}$  feature. To constrain the surface composition of our sampled asteroids and the abundance of silicate material needed to reproduce the weak  $0.9 \mu\text{m}$  band seen on some spectra, we created spatially segregated (geographical) mixtures of several terrestrial and meteoritic materials in different grain sizes. We considered endmembers from among all the samples included in the US Geological Digital Spectral Library <http://speclab.cr.usgs.gov/spectral-lib.html> and in the RELAB database. The synthetic spectra that we created were compared with the asteroid spectra using the known IRAS albedo and the V+NIR spectral behavior and slope as constraints. A few percent (less than 2%) of orthopyroxenes or hydrated silicates (goethite) added to iron meteorites allowed us to reproduce the weak spectral feature around  $0.9 \mu\text{m}$ . Unfortunately, the synthetic spectra did not match both albedo, spectral slope, and band depth and center of the observed asteroids. Moreover, synthetic spectra do not give unique results, as we can obtain similar spectra by adding more components or changing the grain size properties of minerals.

[HERE FIGURE 10]

In Fig. 10 we show an example of two different mixtures proposed for the asteroid 22 Kalliope. The solid line represents a mixture with 98% pallasite (RE-LAB file ckmb43) and 2% goethite, the dashed line shows a mixture of the same meteorite enriched with 1% of orthopyroxene (grain size of 25–45  $\mu\text{m}$ ). The spectral behaviour of both mixtures does not completely match all the spectral characteristics of 22 Kalliope. Figure 10 emphasizes our results that a) it is not easy to fully reproduce the 0.9  $\mu\text{m}$  band, asteroid albedo and spectral slope simply enriching an iron meteorite with some silicates, b) the 0.9  $\mu\text{m}$  band could be reproduced both with a small amount of anhydrous silicates such as orthopyroxene, but also with some hydrated silicates like goethite. This last possibility cannot be completely ruled out. It would support the hypothesis of the presence of hydrated materials on some M-type asteroids, as inferred by Rivkin et al. (1995; 2000) with the detection of the 3  $\mu\text{m}$  band.

Cloutis et al. (1990) identified the 0.9  $\mu\text{m}$  feature in the spectra of some enstatite chondrites. However, the shape of the spectra in our study is similar to iron meteorites, which are featureless. Feierberg et al. (1982) have shown that the physical state of the surface plays an important role in the relative contribution of metal to the spectrum of a silicate-metal mixture. If the surface is spotty with separate areas of pure silicate and pure metal, the spectrum differs very little from that of pure silicate, even in the case of 50% metal content. But if metal and pyroxene particles were mixed, the presence of 50% metal almost completely suppresses the pyroxene bands and the spectrum appears to be indistinguishable from that of the pure metal. Thus, our spectra could have a fairly high concentration of silicate materials, as long as the surface composition is well-mixed.

The results of our search for meteorite analogs confirm that these objects originally in the Tholen M-class could be the parent bodies both of iron (or stony-iron) meteorites and enstatite chondrites. Note that the enstatite chondrites were supposed to have formed close to the Sun (1-1.4 AU) (Shukolyukov and Lugmair 2004). Together with aubrites, enstatite chondrites are the only group of meteorites that have the same oxygen isotopic composition as the Earth–Moon system (Clayton et al. 1984). It is excluded that the parent bodies of enstatite chondrites still reside so close to the Sun, but they may have been scattered into the main belt ( $\sim 2.2\text{--}3.0$  AU), as described by the Bottke et al.(2006) migration scenario. The same hypothesis has been proposed by Bottke et al. (2006) for iron meteorites, that is iron meteorite parent bodies that formed in the terrestrial planet region with fast accretion times. This allowed small planetesimals to melt early in Solar System history by the decay of short-lived radionuclides, then be scattered in the main

belt.

## 8. Conclusions

We observed and analyzed spectra obtained in the visible and near infrared wavelength range (0.4-2.5  $\mu\text{m}$ ) of 30 asteroids selected according to their original classifications as M-types, following the Tholen (1984) taxonomy. The results of our investigation are the following:

- Tholen M-type asteroids show a large variety of spectral behaviors when their spectral coverage is extended into the near-infrared.
- Several weak absorption bands have been identified in extending the spectral range for objects defined as Tholen M-types, showing that their surface compositions are not exclusively metallic. In particular on several asteroids we identify a weak feature (1-5 % depth) in the 0.9  $\mu\text{m}$  wavelength region attributed to low-Fe, low-Ca orthopyroxene minerals. All these asteroids belong to the Xk class in the Bus-DeMeo taxonomy. Some asteroids show a band at 0.43  $\mu\text{m}$  (16 Psyche, 22 Kalliope, 69 Hesperia, 216 Kleopatra, 338 Budrosa, and 498 Tokio) that can be attributed to chlorites and Mg-rich serpentines, or to pigeonite or augite, or to an  $\text{Fe}^{3+}$  spin-forbidden transition in the iron sulfate jarosite. 132 Aethra shows a 0.49  $\mu\text{m}$  band typical of the Xe type (following the Bus & Binzel (2002b) taxonomy) probably due to sulfides such as oldhamite and/or troilite. 135 Hertha has a faint band at  $\sim 0.51 \mu\text{m}$  similar to the  $\text{Fe}^{2+}$  spin-forbidden crystal field transitions in Earth and lunar pyroxene. The spectrum of 755 Quintilla is peculiar with four absorption bands: 0.9 and 1.9  $\mu\text{m}$  features could be attributed to pyroxene silicates, but the origins of the 1.37 and 1.61  $\mu\text{m}$  bands are unknown.
- A comparison with the published literature reveals that at least 4 asteroids (129 Antigone, 325 Heidelberga, 498 Tokio, and 785 Zwetana) display surface variability. Seven additional objects here investigated (16 Psyche, 201 Penelope, 250 Bettina, 369 Aeria, 516 Amherstia, 558 Carmen, and 755 Quintilla) have slightly different spectral slope values or band center positions as compared to the data already published in the literature. These variations may be real but we cannot exclude that they are simply due to the observational uncertainties or to different data acquisition and reduction processes.

- We performed a search of meteorite and/or mineral spectral matches between our asteroid sample and the RELAB database. We confirm that these objects could be the parent bodies both of iron (or stony-iron) meteorites and enstatite chondrites, as suggested in the literature. Only 498 Tokio, which has an anomalous low albedo value (7%) within the Tholen definition for the M-type population, is best matched by a CV carbonaceous chondrite.
- Our attempt to model the asteroid spectra with mixtures of iron/stony iron meteorites enriched with a few percent silicates did not match the albedo and spectral characteristics of our sample. The amount of silicates needed to reproduce the weak  $0.9 \mu\text{m}$  feature seen on some asteroids is very small, less than 2%.
- A statistical analysis of our sampled asteroids' spectral characteristics versus orbital elements and physical parameters indicated a possible correlation between the continuum slope and semi-major axis, and two anti-correlations between visible slope to albedo and continuum slope to rotational period. Our asteroid sample derived from the Tholen M-type tends to be dark in albedo and red in near infrared slope with increasing value of the semi-major axis. Fast M-type rotators tend to be redder than slow rotators.

### **Acknowledgments**

We thank Prof R. Binzel and an anonymous referee for their very useful comments that help us improving the paper. We thank Dr. F. DeMeo for her help in the classification of the observed asteroids in her taxonomy. Taxonomic-type results presented in this work were determined in part using a Bus-DeMeo Taxonomy Classification Web tool developed by Stephen M. Slivan at MIT with the support of National Science Foundation Grant 0506716 and NASA Grant NAG5-12355. This research utilizes spectra acquired with the NASA RELAB facility at Brown University. This paper is in part based on observations made with the Italian Telescopio Nazionale Galileo (TNG) operated on the island of La Palma by the Centro Galileo Galilei of the INAF (Istituto Nazionale di Astrofisica) at the Spanish Observatorio del Roque de los Muchachos of the Instituto de Astrofisica de Canarias. BEC thanks the Observatoire de Paris for kind hospitality during her sabbatic from Ithaca College in the Spring of 2009.

### **References**

Adams, J. B. 1975. Interpretation of visible and near-infrared reflectance spectra

of pyroxenes other rock-forming minerals. In *Infrared and Raman Spectroscopy of Lunar and Terrestrial Minerals* (C. Karr, Jr., Ed.), pp. 901-16. Academic Press, New York

Baffa, C., Comoretto, G., Gennari, S., Lisi, F., Oliva, E., Biliotti, V., Checucci, A., Gavrioussév, V., Giani, E., Ghinassi, F., Hunt, L. K., Maiolino, R., Mannucci, F., Marcucci, G., Sozzi, M., Stefanini, P., Testi, L., 2001. NICS: The TNG Near Infrared Camera Spectrometer. *Astron. Astroph.* 378, 722-728

Bell, J.F., Davis, D., Hartmann, W.K., Gaffey, M.J., 1989. Asteroids: The big picture. In: Binzel, R.P., Gehrels, T., Matthews, M.S. (Eds.), *Asteroids II*. Univ. of Arizona Press, Tucson, pp. 921-948

Belskaya, I. N., Lagerkvist, C.I., 1996. Physical properties of M class asteroids. *Planet. Space Sci.* 44, 783-794

Birlan, M., Vernazza, P., Nedelcu, D. A., 2007. Spectral properties of nine M-type asteroids. *Astron. Astroph.* 475, 747-754

Binzel, R. P., Bus, S. J., Sunshine, J., and Burbine, T. H., 1995. Rotationally Resolved Spectra of Asteroid 16 Psyche. *Icarus* 117, 443-445

Bottke, W.F., Nesvorn, D., Grimm, R.E., Morbidelli, A., O'Brien, D.P., 2006. Iron meteorites as remnants of planetesimals formed in the terrestrial planet region. *Nature* 439, 821-824

Britt, D.T., Pieters, C. M., 1988. Bidirectional reflectance properties of iron-nickel meteorites. In: *Lunar and Planetary Science Conference*, 503-512.

Britt, D.T., Yeomans, D., Housen, K., Consolmagno, G., 2002. Asteroid density, porosity, and structure. In: Bottke Jr., W.F., Cellino, A., Paolicchi, P., Binzel, R.P. (Eds.), *Asteroids III*. Univ. of Arizona, Tucson, pp. 485-500

Burbine, T. H., Cloutis, E. A., Bus, S. J., Meibom, A., Binzel, R. P., 1998. The detection of troilite (FeS) on the surfaces of E-class asteroids. *Bull. Am. Astron. Soc.* 30, 711

Burbine, T. H., McCoy, T. J., Nittler, L., Benedix, G., Cloutis, E., Dickenson, T. 2002a. Spectra of extremely reduced assemblages: Implications for Mercury. *Meteorit. Planet. Sci.* 37, 1233-1244

Burbine, T.H., McCoy, T.J., Meibom, A., 2002b. Meteorite parent bodies, in *Asteroids III*, Bottke, W. et al. Editors, Univ. of Arizona Press, Tucson.

Burns, R. G., D. J. Vaughan, R. M. Abu-Eid, M. Witner, and A. Morawski 1973. Spectral evidence for Cr<sup>3+</sup>, Ti<sup>3+</sup>, and Fe<sup>2+</sup> rather than Cr<sup>2+</sup>, and Fe<sup>3+</sup> in lunar ferromagnesian silicates. In *Proc. 4th Lunar Sci. Conf.* 983-994

Bus, S. J., Binzel, R. P., 2002a. Phase II of the Small Main-Belt Asteroid Spectroscopic Survey: The Observations. *Icarus* 158, 106-145

- Bus, S. J., Binzel, R. P., 2002b. Phase II of the Small Main-Belt Asteroid Spectroscopic Survey: A Feature-Based Taxonomy. *Icarus* 158, 146-177
- Bus, S.J., Binzel, R.P., Volquardsen, E., 2003. Characterizing the visible and near-IR spectra of asteroids using principal component analysis. *Bull. Amer. Astron. Soc.* 35, 976 (abstract)
- Busarev, V. V., 1998. Spectral Features of M-Asteroids: 75 Eurydike and 201 Penelope. *Icarus*, 131, 32–40
- Chapman, C. R., Gaffey, M. J., 1979. Spectral reflectances of the asteroids. In *Asteroids* (Gehrels, Ed.), pp. 1064-1089. Univ. of Arizona Press, Tucson
- Clayton, R.N., Mayeda, T.K., Rubin, A.E., 1984. Oxygen isotopic compositions of enstatite chondrites and aubrites. In: *Proc. 15th Lunar Planet. Sci. Conf.* *J. Geophys. Res. Suppl.* 89, C245C249
- Clark, B. E., Bus, S. J., Rivkin, A. S., Shepard, M. K., Shah, S., 2004a. Spectroscopy of X-Type Asteroids. *Astron. J* 128, 3070-3081
- Clark, B.E., Bus, S.J., Rivkin, A.S., McConnochie, T., Sander, J., Shah, S., Hiroi, T., Shepard, M., 2004b. E-Type asteroid spectroscopy and compositional modeling, *JGR* 109, 1010-1029
- Clark, B.E., Ockert-Bell, M.E., Cloutis, E.A., Nesvorny, D., Moth-Diniz, T., and Bus, S.J. 2009. Spectroscopy of K-complex Asteroids: Parent Bodies of Carbonaceous Meteorites? *Icarus* 202, 119-133
- Clark, B.E., Ziffer, J., Nesvorny, D., Campins, H., Rivkin, A.S., Hiroi, T., Barucci, M.A., Fulchignoni, M., Binzel, R.P., Fornasier, S., DeMeo, F., Ockert-Bell, M.E., Licandro, J., and Moth-Diniz, T., 2010. Spectroscopy of B-type Asteroids: Subgroups and Meteorite Analogs. *JGR Planets*, in press
- Cloutis, E. A., Gaffey, M. J., Smith, D. G. W., Lambert, R. St. J., 1990. Metal Silicate Mixtures: Spectral Properties and Applications to Asteroid Taxonomy. *J. Geophys. Res.*, 95, 281, 83238338
- Cloutis, E. A., and T. H. Burbine 1999. The spectral properties of troilite/pyrrhotite and implications for the E-asteroids. *Lunar and Planet. Sci. Conf. XXX*, 1875
- Cloutis, E.A., Hardersen, P.S., Bish, D.L., Bailey, D.T., Gaffey, M.J., Craig, M.A., 2010. Reflectance spectra of iron meteorites: Implications for spectral identification of their parent bodies. *Meteoritics and Planetary Science*, in press.
- Descamps, P., Marchis, F., Pollock, J., Berthier, J., Vachier, F., Birlan, M., Kaasalainen, M., Harris, A. W., Wong, M. H., Romanishin, W. J., Cooper, E. M., Kettner, K. A., Wiggins, P., Kryszczyńska, A., Polinska, M., Coliac, J.F., Devyatkin, A., Verestchagina, I., Gorshonov, D., 2008. New determination of the size and bulk density of the binary Asteroid 22 Kalliope from observations of mutual eclipses. *Icarus* 196, 578-600

- DeMeo, F. E., Binzel, R. P., Slivan, S. M., Bus, S. J., 2009. An extension of the Bus asteroid taxonomy into the near-infrared. *Icarus* 202, 160-180
- D'Odorico, S., 1990. EMMI, the ESO multi-mode instrument, successfully installed at the NTT. *The Messenger* 61, 51-56
- Feierberg, M. A., Larson, H.P., Chapman, C. R., 1982. Spectroscopic evidence for undifferentiated S-type asteroids. *Astrophys. J.* 257, 361-372
- Fieber-Beyer, S. K., Gaffey, M. J., Hardersen, P. S., 2006. Near-Infrared Spectroscopic Analysis of Mainbelt M-Asteroid 755 Quintilla. 37th Annual Lunar and Planetary Science Conference, March 13-17, 2006, League City, Texas, abstract no.1315
- Fornasier, S., Dotto, E., Marzari, F., Barucci, M.A., Boehnhardt, H., Hainaut, O., de Bergh, C., 2004a. Visible spectroscopic and photometric survey of L5 Trojans : investigation of dynamical families. *Icarus* 172, 221–232
- Fornasier, S., Dotto, E., Barucci, M. A., Barbieri, C., 2004b. Water ice on the surface of the large TNO 2004 DW. *Astron. Astroph.* 422, L43-L46
- Fornasier, S., Marzari, F., Dotto, E., Barucci, M. A., Migliorini, A., 2007. Are the E-type asteroids (2867) Steins, a target of the Rosetta mission, and NEA (3103) Eger remnants of an old asteroid family? *Astron. Astroph.* 474, 29-32
- Fornasier, S., Migliorini, A., Dotto, E., Barucci, M. A., 2008. Visible and near infrared spectroscopic investigation of E-type asteroids, including 2867 Steins, a target of the Rosetta mission. *Icarus* 196, 119–134
- Gaffey, M. J., Burbine, T. H., Piatek, J. L., Reed, K. L., Chaky, D. A., Bell J. F. Brown, R. H., 1993. Mineralogical variations within the S-type asteroid class. *Icarus* 106, 573–602
- Gaffey, M. J., 1976. Spectral reflectance characteristics of the meteorite classes. *J. Geophys. Res.* 81, 905–920
- Hardersen, P. S., Gaffey, M. J., Abell, P. A., 2005. Near-IR spectral evidence for the presence of iron-poor orthopyroxenes on the surfaces of six M-type asteroids. *Icarus* 175, 141–158
- Hardersen, P. S., Gaffey, M. J., Cloutis, E., Abell, P. A., Reddy, V., 2006a. Discovering Spectral and Mineralogical Diversity Among the M-Asteroid Population. 37th Annual Lunar and Planetary Science Conference, 2006, League City, Texas, abstract no. 1106
- Hardersen, P. S., Gaffey, M. J., Abell, P. A., 2006b. Near-infrared Reflectance Spectra Of 135 Hertha, 224 Oceana, 516 Amherstia, And 872 Holda. *Bulletin of the American Astronomical Society*, Vol. 38, p.626
- Hardersen, P. S., Gaffey, M. J., Kumar, S., 2007a. Nir Spectra And Interpretations For M-asteroids 369 Aeria And 785 Zwetana. *Bulletin of the American*

Astronomical Society, Vol. 39, p . 478

Hardersen, P. S., Gaffey, M. J., Kumar, S., Fieber-Beyer, S. K., Crowell, J. J., Crowell, A. M., 2007b. Near-IR Reflectance Spectra of M-Asteroids 250 Bettina, 369 Aeria, 413 Edburga, and 931 Whitemora. 38th Lunar and Planetary Science Conference, March 12-16, 2007 in League City, Texas. LPI Contribution No. 1338, p.1956

Hazen, R. M., P. M. Bell, and H. K. Mao 1978. Effects of compositional variation on absorption spectra of lunar pyroxenes. In Proc. 9th Lunar Planet. Sci. Conf., 29192934.

Jones, T. D., Lebofsky, L. A., Lewis, J. S., Marley, M. S., 1990. The composition and origin of the C, P, and D asteroids: Water as a tracer of thermal evolution in the outer belt. *Icarus*, 88, 172192

King, T.V.V., Clark, R.N., 1989. Spectral characteristics of chlorites and Mgserpentines using high resolution reflectance spectroscopy. *J. Geophys. Res.* 94, 1399714008

Kochetova, O.M., 2003. Application of new criteria for selecting perturbed minor planets for determination of masses of perturbing minor planets by dynamical method. In: Reports of Inst. of Applied Astronomy of Russian Acad. Sci. No. 165, St. Petersburg, 42 pp. (in Russian).

Lazzarin, M., Marchi, S., Moroz, L. V., Brunetto, R., Magrin, S., Paolicchi, P., Strazzulla, G., 2006. Space Weathering in the Main Asteroid Belt: The Big Picture. *Astrophysical J.* 647, 179-182

Lord, S., 1992. A New Software Tool for Computing Earth's Atmospheric Transmission of Near- and Far-Infrared Radiation. NASA Technical Memorandum 103957

Lupisko, D. F., Belskaya, I. N., 1989. On the surface composition of the M-type asteroids. *Icarus* 78, 395–401

Magri, C. Nolan, M. C.; Ostro, S. J., Giorgini, J. D., 2007. A radar survey of main-belt asteroids: Arecibo observations of 55 objects during 1999 2003. *Icarus* 186, 126–151

Margot, J.-L., Brown, M.E., 2003. A low-density M-type asteroid in the main-belt. *Science* 300, 19391942

Moorwood, A., Cuby, J.-G., Lidman, C., 1998. SOFI sees first light at the NTT. *The Messenger* 91, 9-13

Moth-Diniz, T., J.M. Carvano, S.J. Bus, R. Duffard, T. Burbine, 2008. Mineralogical analysis of the Eos family from near-infrared spectra. *Icarus* 195, 277-294

Ockert-Bell, M.E., Clark, B.E., Shepard, M.K., Rivkin, A.S., Binzel, R.P., Thomas, C.A., DeMeo, F.E., Bus, S.J., Shah, S., 2008. Observations of X/M

asteroids across multiple wavelengths. *Icarus* 195 (1), 206219

Ostro, S. J., Campbell, D. B., Chandler, J. F., Hine, A. A., Hudson, R. S., Rosema, K. D., Shapiro, I. I., 1991. Asteroid 1986 DA: Radar evidence for a metallic composition. *Science*, 252, 1399–1404

Ostro, S. J., Hudson, R. S., Nolan, M. C., Margot, J. L., Scheeres, D. J., Campbell, D. B., Magri, C., Giorgini, J. D., Yeomans, D. K., 2000. Radar observations of asteroid 216 Kleopatra. *Science*, 288, 836839

Pieters, C. 1983. Strength of mineral absorption features in the transmitted component of near-infrared reflected light: First results from RELAB, *J. Geophys. Res.*, 88, 9534–9544

Rayner, J.T., Toomey, D., Onaka, P., Denault, A., Stahlberger, W., Vacca, W., Cushing, M., 2003. SpeX: A Medium-Resolution 0.8-5.5 m Spectrograph and Imager for the NASA Infrared Telescope Facility. *Pub. Astron. Soc. Pacific*, 115 (805), 362-382

Rivkin, A. S., Howell, E. S., Britt, D. T., Lebofsky, L. A., Nolan, M. C., Branston, D. D., 1995. 3-m spectrophotometric survey of M- and E-class asteroids. *Icarus*, 117, 90–100

Rivkin, A.S., Howell, E.S., Lebofsky, L.A., Clark, B.E., Britt, D.T., 2000. The nature of M-class asteroids from 3-m observations. *Icarus* 145, 351–368

Rivkin, A. S., Howell, E. S., Vilas, F., Lebofsky L. A., 2002. Hydrated minerals on asteroids: The astronomical record. In *Asteroids III*, Bottke W. et al. editors, Univ. of Arizona, Tucson, pp 235–253

Shepard, M. K., Clark, B. E., Nolan, M. C., Howell, E. S., Magri, C., Giorgini, J. D., Benner, L. A. M., Ostro, S. J., Harris, A. W., Warner, B., et al., 2008. A radar survey of M- and X-class asteroids. *Icarus* 195, 184–205

Shukolyukov, A., Lugmair, G.W., 2004. Manganese-chromium isotope systematics of enstatite meteorites. *Geochim. Cosmochim. Acta* 68, 28752888

Spearman, C. 1904. The proof and measurements of associations between two things. *AM. J. Psychol.* 57, 72

Sunshine, J. M., Shelte, S. J., McCoy, T. J., Burbine, T. H., Corrigan, C. M., Binzel, R. P., 2004. Highcalcium pyroxene as an indicator of igneous differentiation in asteroids and meteorites. *Meteoritics and Planetary Sci.* 39, 1343-1357

Takir, D., Hardersen, P. S., Gaffey, M. J., 2008. The Near-Infrared Spectroscopy of Two M-Class Main Belt Asteroids, 77 Frigga and 325 Heidelberg. 39th Lunar and Planetary Science Conference, League City, Texas. LPI Contribution No. 1391., p.1084

Taylor, S. R., 1992. Solar system evolution: a new perspective. an inquiry into the chemical composition, origin, and evolution of the solar system. In *Solar*

System evolution: A new Perspective, Cambridge Univ. Press.

Tedesco, E.F., P.V. Noah, M. Moah, and S.D. Price, 2002. The supplemental IRAS minor planet survey. *The Astronomical Journal* 123, 10565-10585

Tholen, D.J., 1984. Asteroid taxonomy from cluster analysis of photometry. Ph.D. dissertation, University of Arizona, Tucson

Tholen, D.J., Barucci, M.A., 1989. Asteroids taxonomy. In: Binzel, R.P., Gehrels, T., Matthews, M.S. (Eds.), *Asteroids II*. Univ. of Arizona Press, Tucson, pp. 298–315

Vernazza, P., Brunetto, R., Binzel, R. P., Perron, C., Fulvio, D., Strazzulla, G., Fulchignoni, M., 2009. Plausible parent bodies for enstatite chondrites and mesosiderites: Implications for Lutetia's fly-by. *Icarus* 202, 477-486

Viateau, B., 2000. Mass and density of Asteroids (16) Psyche and (121) Hermione. *Astron. Astrophys.* 354, 725731

Vilas, F., Hatch, E.C., Larson, S.M., Sawyer, S.R., Gaffey, M.J., 1993. Ferric iron in primitive asteroids: a 0.43  $\mu$ m absorption feature. *Icarus* 102, 225-231

Vilas, F., 1994. A cheaper, faster, better way to detect water of hydration on Solar System bodies. *Icarus* 111, 456-467

## Tables

**Table 1.** Observational circumstances for the observed sample, for which their visible wavelength spectra and albedos all satisfy the definition of M-type in the Tholen taxonomy. Solar analog stars named "hip" come from the Hipparcos catalogue, "la" from the Landolt photometric standard stars catalogue, and "HD" from the Henry Draper catalogue

| Object         | Night      | UT <sub>start</sub> | T <sub>exp</sub> | Tel. | Instr.  | Grism | airm. | Solar Analog (airm.)  |
|----------------|------------|---------------------|------------------|------|---------|-------|-------|---|
| 16 Psyche      | 15 Nov. 04 | 19:31               | 40               | TNG  | Dolores | LR-R  | 1.46  | la115-271 (1.31)  |
| 16 Psyche      | 15 Nov. 04 | 19:33               | 60               | TNG  | Dolores | MR-B  | 1.47  | la115-271 (1.32)  |
| 16 Psyche      | 18 Nov. 04 | 19:21               | 80               | TNG  | NICS    | Amici | 1.45  | la93-101 (1.34)   |
| 22 Kalliope    | 13 Aug. 05 | 07:35               | 120              | NTT  | EMMI    | GR1   | 1.02  | HD1835 (1.07)   |
| 22 Kalliope    | 21 Dec. 07 | 14:46               | 1800             | IRTF | SPEX    | Prism | 1.24  | hyades64(1.00),la115-270(1.10),<br>la93-101(1.10), la102-1081(1.10)   |
| 55 Pandora     | 25 May 04  | 10:33               | 60               | NTT  | EMMI    | GR1   | 1.31  | la112-1333 (1.17)   |
| 55 Pandora     | 17 Sep. 05 | 11:37               | 1920             | IRTF | SPEX    | Prism | 1.10  | hyades64 (1.00),la115-270(1.10),<br>la93-101(1.10), la112-1333(1.10)  |
| 55 Pandora     | 20 Sep. 05 | 13:56               | 1000             | IRTF | SPEX    | Prism | 1.00  | la110-361(1.10),la115-270(1.10),<br>.la93-101(1.10), la112-1333(1.10) |
| 69 Hesperia    | 18 Nov. 04 | 06:34               | 120              | TNG  | Dolores | LR-R  | 1.12  | hyades64 (1.4)  |
| 69 Hesperia    | 18 Nov. 04 | 06:37               | 180              | TNG  | Dolores | MR-B  | 1.13  | hyades64 (1.4)  |
| 69 Hesperia    | 19 Nov. 04 | 06:01               | 480              | TNG  | NICS    | Amici | 1.16  | la98-978 (1.21)   |
| 97 Klotho      | 20 Jan 07  | 03:12               | 20               | NTT  | EMMI    | GR1   | 1.24  | la98-978 (1.22)   |
| 97 Klotho      | 20 Sep. 05 | 06:06               | 960              | IRTF | SPEX    | Prism | 1.20  | la110-361(1.10),la115-270(1.10),<br>la93-101(1.10), la112-1333(1.10)  |
| 97 Klotho      | 17 Dec 06  | 06:06               | 670              | IRTF | SPEX    | Prism | 1.1   | hyades64 (1.15)   |
| 97 Klotho      | 19 Dec 06  | 10:48               | 600              | IRTF | SPEX    | Prism | 1.1   | hyades64 (1.15), la102-1081 (1.1)                                     |
| 110 Lydia      | 16 Nov. 04 | 05:24               | 180              | TNG  | Dolores | LR-R  | 1.12  | HD28099 (1.05)  |
| 110 Lydia      | 16 Nov. 04 | 05:28               | 180              | TNG  | Dolores | MR-B  | 1.11  | HD28099 (1.05)  |
| 110 Lydia      | 19 Nov. 04 | 05:03               | 360              | TNG  | NICS    | Amici | 1.14  | la98-978 (1.17)   |
| 125 Liberatrix | 20 Nov. 04 | 20:37               | 180              | TNG  | Dolores | LR-R  | 1.22  | la115-271 (1.16)  |
| 125 Liberatrix | 20 Nov. 04 | 20:41               | 180              | TNG  | Dolores | MR-B  | 1.21  | la115-271 (1.16)  |
| 125 Liberatrix | 20 Nov. 04 | 22:01               | 150              | TNG  | Dolores | LR-R  | 1.12  | la115-271 (1.16)  |
| 125 Liberatrix | 20 Nov. 04 | 22:05               | 150              | TNG  | Dolores | MR-B  | 1.12  | la115-271 (1.16)  |
| 125 Liberatrix | 20 Nov. 04 | 23:27               | 180              | TNG  | Dolores | LR-R  | 1.18  | la115-271 (1.16)  |
| 125 Liberatrix | 20 Nov. 04 | 23:31               | 180              | TNG  | Dolores | MR-B  | 1.19  | la115-271 (1.16)  |
| 129 Antigone   | 13 Aug 05  | 00:07               | 60               | NTT  | EMMI    | GR1   | 1.16  | la112-1333 (1.19)   |
| 129 Antigone   | 14 Aug 05  | 02:21               | 160              | NTT  | SOFI    | GBF   | 1.81  | la107-684 (2.03)  |
| 129 Antigone   | 14 Aug 05  | 02:25               | 200              | NTT  | SOFI    | GRF   | 1.85  | la107-684 (2.03)  |
| 132 Aertha     | 25 May 04  | 10:45               | 180              | NTT  | EMMI    | GR1   | 1.43  | la112-1333 (1.17)   |
| 135 Hertha     | 26 May 04  | 09:58               | 120              | NTT  | EMMI    | GR1   | 1.27  | la112-1333 (1.18)   |
| 135 Hertha     | 07 Nov. 08 | 10:28               | 630              | IRTF | SPEX    | Prism | 1.00  | hyades64 (1.10), la93-101(1.20),<br>la97-249(1.10)                    |
| 135 Hertha     | 08 Nov. 08 | 10:51               | 400              | IRTF | SPEX    | Prism | 1.00  | hyades64 (1.10), la97-249(1.10)                                       |
| 135 Hertha     | 22 Dec. 08 | 06:35               | 870              | IRTF | SPEX    | Prism | 1.05  | hyades64(1.05), la93-101(1.10)  |
| 161 Athor      | 12 Aug 05  | 04:29               | 160              | NTT  | SOFI    | GBF   | 1.06  | hip096165 (1.09)  |
| 161 Athor      | 12 Aug 05  | 04:34               | 160              | NTT  | SOFI    | GRF   | 1.07  | hip096165 (1.09)  |
| 161 Athor      | 13 Aug 05  | 02:47               | 150              | NTT  | EMMI    | GR1   | 1.01  | HD144585 (1.22)   |
| 201 Penelope   | 29 Feb. 04 | 00:32               | 90               | TNG  | Dolores | LR-R  | 1.15  | hd89010 (1.02)  |
| 201 Penelope   | 29 Feb. 04 | 00:35               | 90               | TNG  | Dolores | LR-B  | 1.16  | hd89010 (1.18)  |
| 216 Kleopatra  | 18 Nov. 04 | 05:25               | 90               | TNG  | Dolores | LR-R  | 1.09  | la98-978 (1.20)   |
| 216 Kleopatra  | 18 Nov. 04 | 05:28               | 90               | TNG  | Dolores | MR-B  | 1.09  | la98-978 (1.20)   |
| 216 Kleopatra  | 19 Nov. 04 | 04:45               | 180              | TNG  | NICS    | Amici | 1.10  | la98-978 (1.17)   |
| 224 Oceana     | 15 Nov. 04 | 21:24               | 240              | TNG  | Dolores | LR-R  | 1.08  | hyades64 (1.03)   |
| 224 Oceana     | 15 Nov. 04 | 21:29               | 240              | TNG  | Dolores | MR-B  | 1.08  | hyades64 (1.03)   |
| 224 Oceana     | 20 Sep. 05 | 15:20               | 960              | IRTF | SPEX    | Prism | 1.20  | la110-361(1.10), la115-270(1.10),<br>la93-101(1.1), la112-1333(1.1)   |
| 250 Bettina    | 18 Nov. 04 | 06:46               | 120              | TNG  | Dolores | LR-R  | 1.04  | hyades64 (1.40)   |

Continued on next page

| Object          | Night      | UT <sub>start</sub> | T <sub>exp</sub> | Tel. | Instr.  | Grism | airm. | Solar Analog (airm.)                                |
|-----------------|------------|---------------------|------------------|------|---------|-------|-------|---|
| 250 Bettina     | 18 Nov. 04 | 06:49               | 120              | TNG  | Dolores | MR-B  | 1.05  | hyades64 (1.40)                                     |
| 250 Bettina     | 21 Nov. 04 | 06:41               | 80               | TNG  | NICS    | Amici | 1.04  | la98-978 (1.17)                                     |
| 325 Heidelberga | 20 Nov. 04 | 01:42               | 60               | TNG  | Dolores | LR-R  | 1.15  | hyades64 (1.02)                                     |
| 325 Heidelberga | 20 Nov. 04 | 01:45               | 120              | TNG  | Dolores | MR-B  | 1.16  | hyades64 (1.02)                                     |
| 325 Heidelberga | 19 Nov. 04 | 00:24               | 600              | TNG  | NICS    | Amici | 1.02  | hyades64 (1.03)                                     |
| 338 Budrosa     | 13 Aug 05  | 01:17               | 360              | NTT  | EMMI    | GR1   | 1.10  | HD144585 (1.05)                                     |
| 338 Budrosa     | 12 Aug 05  | 01:40               | 360              | NTT  | SOFI    | GBF   | 1.14  | hip083805 (1.23)                                    |
| 338 Budrosa     | 12 Aug 05  | 02:10               | 280              | NTT  | SOFI    | GRF   | 1.22  | hip083805 (1.23)                                    |
| 347 Pariana     | 13 Aug 05  | 06:57               | 420              | NTT  | EMMI    | GR1   | 1.02  | HD1835 (1.07)                                       |
| 347 Pariana     | 12 Aug 05  | 07:30               | 480              | NTT  | SOFI    | GBF   | 1.04  | hip103579 (1.06)                                    |
| 347 Pariana     | 12 Aug 05  | 07:39               | 480              | NTT  | SOFI    | GRF   | 1.05  | hip103579 (1.06)                                    |
| 369 Aeria       | 13 Aug 05  | 01:08               | 240              | NTT  | EMMI    | GR1   | 1.07  | HD144585 (1.05)                                     |
| 369 Aeria       | 12 Aug 05  | 02:49               | 240              | NTT  | SOFI    | GBF   | 1.33  | hip083805 (1.23)                                    |
| 369 Aeria       | 12 Aug 05  | 02:56               | 280              | NTT  | SOFI    | GBF   | 1.36  | hip083805 (1.23)                                    |
| 382 Dodona      | 13 Aug 05  | 00:34               | 300              | NTT  | EMMI    | GR1   | 1.45  | HD144585 (1.22)                                     |
| 418 Alemania    | 20 Jan 07  | 09:05               | 360              | NTT  | EMMI    | GR1   | 1.13  | la98-978 (1.22)                                     |
| 441 Bathilde    | 13 Aug 05  | 05:58               | 180              | NTT  | EMMI    | GR1   | 1.21  | HD1835 (1.07)                                       |
| 441 Bathilde    | 12 Aug 05  | 04:54               | 280              | NTT  | SOFI    | GBF   | 1.10  | hip096165 (1.09)                                    |
| 441 Bathilde    | 12 Aug 05  | 05:01               | 280              | NTT  | SOFI    | GRF   | 1.10  | hip096165 (1.09)                                    |
| 498 Tokio       | 13 Aug 05  | 05:45               | 60               | NTT  | EMMI    | GR1   | 1.10  | HD1835 (1.07)                                       |
| 498 Tokio       | 12 Aug 05  | 05:37               | 120              | NTT  | SOFI    | GBF   | 1.07  | hip103572 (1.06)                                    |
| 498 Tokio       | 12 Aug 05  | 05:40               | 160              | NTT  | SOFI    | GBF   | 1.08  | hip103572 (1.06)                                    |
| 516 Amherstia   | 19 Nov. 04 | 00:07               | 360              | TNG  | NICS    | Amici | 1.20  | la98-978 (1.17)                                     |
| 516 Amherstia   | 20 Jan 07  | 09:23               | 60               | NTT  | EMMI    | GR1   | 1.07  | la102-1081 (1.22)                                   |
| 558 Carmen      | 13 Aug 05  | 00:50               | 480              | NTT  | EMMI    | GR1   | 1.49  | HD144585 (1.22)                                     |
| 755 Quintilla   | 13 Aug 05  | 02:32               | 600              | NTT  | EMMI    | GR1   | 1.08  | HD144585 (1.07)                                     |
| 755 Quintilla   | 14 Aug 05  | 02:56               | 600              | NTT  | SOFI    | GBF   | 1.03  | hip99046 (1.01)                                     |
| 755 Quintilla   | 14 Aug 05  | 03:19               | 960              | NTT  | SOFI    | GRF   | 1.05  | hip99046 (1.01)                                     |
| 785 Zwetana     | 29 Feb. 04 | 22:06               | 240              | TNG  | Dolores | LR-R  | 1.46  | la102-1081 (1.34)                                   |
| 785 Zwetana     | 1 Mar. 04  | 22:02               | 960              | TNG  | NICS    | Amici | 1.39  | hyades64 (1.21)                                     |
| 785 Zwetana     | 12 Aug 05  | 23:03               | 240              | NTT  | EMMI    | GR1   | 1.08  | HD144585 (1.05)                                     |
| 849 Ara         | 15 Nov. 04 | 20:10               | 120              | TNG  | Dolores | LR-R  | 1.09  | HD28099 (1.05)                                      |
| 849 Ara         | 15 Nov. 04 | 20:19               | 120              | TNG  | Dolores | LR-B  | 1.10  | hyades64 (1.03)                                     |
| 849 Ara         | 12 Aug 05  | 09:55               | 480              | NTT  | SOFI    | GBF   | 1.73  | hip11355 (1.49)                                     |
| 849 Ara         | 12 Aug 05  | 10:05               | 480              | NTT  | SOFI    | GRF   | 1.69  | hip11355 (1.49)                                     |
| 860 Ursina      | 20 Nov. 04 | 02:03               | 180              | TNG  | Dolores | LR-R  | 1.15  | hyades64 (1.02)                                     |
| 860 Ursina      | 20 Nov. 04 | 02:07               | 240              | TNG  | Dolores | MR-B  | 1.16  | hyades64 (1.02)                                     |
| 860 Ursina      | 18 Nov. 04 | 22:48               | 480              | TNG  | NICS    | Amici | 1.03  | hyades64 (1.03)                                     |
| 872 Holda       | 20 Nov. 04 | 21:34               | 300              | TNG  | Dolores | LR-R  | 1.18  | la115-271 (1.16)                                    |
| 872 Holda       | 20 Nov. 04 | 21:40               | 300              | TNG  | Dolores | MR-B  | 1.19  | la115-271 (1.16)                                    |
| 872 Holda       | 16 Nov. 05 | 12:51               | 600              | IRTF | SPEX    | Prism | 1.01  | hyades64 (1.15),<br>la115-270(1.10), la93-101(1.20) |

Table 2: Physical and orbital parameters of the M asteroids observed and selected on the basis of the Tholen taxonomy (Tholen, 1984). The Bus and Bus-DeMeo classifications are also reported, together with the spectral slopes value ( $S_{VIS}$  calculated for the 0.55-0.8  $\mu\text{m}$  wavelength range,  $S_{NIR1}$  for the 1.1-1.6  $\mu\text{m}$  range,  $S_{NIR2}$  for the 1.7-2.4  $\mu\text{m}$  range, and  $S_{cont}$  for the whole range).

| Asteroid        | Bus | Bus-DeMeo | albedo | D<br>(Km) | Rot<br>(h) | a<br>(UA) | e      | i<br>( $^{\circ}$ ) | $S_{VIS}$<br>(%/10 $^3$ $\text{\AA}$ ) | $S_{NIR1}$<br>(%/10 $^3$ $\text{\AA}$ ) | $S_{NIR2}$<br>(%/10 $^3$ $\text{\AA}$ ) | $S_{cont}$<br>(%/10 $^3$ $\text{\AA}$ ) |
|-----------------|-----|-----------|--------|-----------|------------|-----------|--------|---------------------|--|---|---|---|
| 16 Psyche       | X   | Xk        | 0.12   | 253.16    | 4.196      | 2.9201    | 0.1395 | 3.1                 | 3.00 $\pm$ 0.54                        | 3.79 $\pm$ 0.93                         | 4.26 $\pm$ 0.84                         | 3.66 $\pm$ 0.71                         |
| 22 Kalliope     | X   | Xk        | 0.14   | 181.00    | 4.148      | 2.9077    | 0.1030 | 13.7                | 3.85 $\pm$ 0.55                        | 2.59 $\pm$ 0.75                         | 1.61 $\pm$ 0.72                         | 2.88 $\pm$ 0.72                         |
| 55 Pandora      | X   | Xk        | 0.30   | 66.70     | 4.804      | 2.7582    | 0.1447 | 7.2                 | 3.19 $\pm$ 0.55                        | 2.25 $\pm$ 0.75                         | 1.90 $\pm$ 0.73                         | 2.25 $\pm$ 0.71                         |
| 69 Hesperia     | X   | Xk        | 0.14   | 138.13    | 5.656      | 2.9776    | 0.1686 | 8.6                 | 4.06 $\pm$ 0.55                        | 2.81 $\pm$ 0.81                         | -1.33 $\pm$ 0.91                        | 3.09 $\pm$ 0.72                         |
| 97 Klotho       | -   | Xc        | 0.23   | 82.83     | 35.15      | 2.6674    | 0.2571 | 11.8                | 3.19 $\pm$ 0.53                        | 1.07 $\pm$ 0.73                         | -0.36 $\pm$ 0.72                        | 1.23 $\pm$ 0.72                         |
| 110 Lydia       | X   | Xk        | 0.18   | 86.09     | 10.92      | 2.7321    | 0.0799 | 5.9                 | 3.94 $\pm$ 0.54                        | 2.75 $\pm$ 0.87                         | 1.21 $\pm$ 0.89                         | 2.88 $\pm$ 0.72                         |
| 125 Liberatrix  | X   | -         | 0.22   | 43.58     | 3.968      | 2.7433    | 0.0807 | 4.6                 | 1.60 $\pm$ 0.55                        | -                                       | -                                       | 1.63 $\pm$ 0.73                         |
| 129 Antigone    | X   | Xc        | 0.16   | 113.00    | 4.957      | 2.8674    | 0.2136 | 12.2                | 3.49 $\pm$ 0.57                        | 0.56 $\pm$ 0.74                         | 1.06 $\pm$ 0.77                         | 0.92 $\pm$ 0.71                         |
| 132 Aethra      | Xe  | -         | 0.20   | 42.87     | 5.168      | 2.6082    | 0.3887 | 25.1                | 2.35 $\pm$ 0.59                        | -                                       | -                                       | 2.83 $\pm$ 0.78                         |
| 135 Hertha      | Xk  | Xk        | 0.14   | 79.24     | 8.400      | 2.4286    | 0.2063 | 2.3                 | 3.22 $\pm$ 0.55                        | 1.87 $\pm$ 0.73                         | 1.25 $\pm$ 0.71                         | 2.07 $\pm$ 0.72                         |
| 161 Athor       | Xc  | Xc        | 0.20   | 44.19     | 7.288      | 2.3805    | 0.1374 | 9.0                 | 2.18 $\pm$ 0.66                        | 1.39 $\pm$ 0.74                         | 0.14 $\pm$ 0.73                         | 1.16 $\pm$ 0.71                         |
| 201 Penelope    | X   | -         | 0.16   | 68.39     | 3.747      | 2.6790    | 0.1809 | 5.7                 | 5.57 $\pm$ 0.57                        | -                                       | -                                       | 5.53 $\pm$ 0.74                         |
| 216 Kleopatra   | Xe  | Xk        | 0.12   | 124.00    | 5.385      | 2.7933    | 0.2521 | 13.1                | 5.40 $\pm$ 0.53                        | 2.96 $\pm$ 0.80                         | 1.94 $\pm$ 0.86                         | 3.36 $\pm$ 0.73                         |
| 224 Oceana      | -   | Xc        | 0.17   | 61.82     | 9.385      | 2.6454    | 0.0455 | 5.8                 | 1.47 $\pm$ 0.56                        | 1.69 $\pm$ 0.79                         | 0.51 $\pm$ 0.74                         | 2.18 $\pm$ 0.71                         |
| 250 Bettina     | Xk  | Xk        | 0.26   | 79.75     | 5.054      | 3.1497    | 0.1245 | 12.8                | 3.79 $\pm$ 0.56                        | 7.00 $\pm$ 0.91                         | 4.22 $\pm$ 0.82                         | 4.83 $\pm$ 0.72                         |
| 325 Heidelberga | -   | X         | 0.11   | 75.72     | 6.737      | 3.204     | 0.1686 | 8.5                 | 5.67 $\pm$ 0.54                        | 3.82 $\pm$ 0.83                         | 2.10 $\pm$ 0.79                         | 4.26 $\pm$ 0.72                         |
| 338 Budrosa     | Xk  | Xk        | 0.18   | 63.11     | 4.6        | 2.9124    | 0.0208 | 6.0                 | 4.15 $\pm$ 0.60                        | 3.11 $\pm$ 0.79                         | 3.29 $\pm$ 0.78                         | 3.12 $\pm$ 0.71                         |
| 347 Pariana     | -   | Xk        | 0.18   | 51.36     | 4.052      | 2.6153    | 0.1639 | 11.7                | 3.66 $\pm$ 0.55                        | 1.86 $\pm$ 0.76                         | 1.97 $\pm$ 0.75                         | 2.32 $\pm$ 0.71                         |
| 369 Aeria       | -   | Xk        | 0.19   | 60.00     | 4.787      | 2.6480    | 0.0985 | 12.7                | 4.48 $\pm$ 0.57                        | 3.18 $\pm$ 0.75                         | 1.92 $\pm$ 0.77                         | 2.75 $\pm$ 0.71                         |
| 382 Dodona      | -   | -         | 0.16   | 58.37     | 4.116      | 3.1183    | 0.1761 | 7.4                 | 5.02 $\pm$ 0.58                        | -                                       | -                                       | 4.76 $\pm$ 0.75                         |
| 418 Alemania    | X   | -         | 0.19   | 34.10     | 4.671      | 2.5919    | 0.1195 | 6.8                 | 4.07 $\pm$ 0.55                        | -                                       | -                                       | 3.39 $\pm$ 0.73                         |
| 441 Bathilde    | Xk  | X         | 0.14   | 70.32     | 10.44      | 2.8049    | 0.0823 | 8.1                 | 5.30 $\pm$ 0.57                        | 2.21 $\pm$ 0.74                         | 0.20 $\pm$ 0.74                         | 2.12 $\pm$ 0.72                         |
| 498 Tokio       | -   | Xc        | 0.07   | 81.83     | 20.00      | 2.6513    | 0.2245 | 9.5                 | 5.76 $\pm$ 0.57                        | 0.06 $\pm$ 0.75                         | 0.20 $\pm$ 0.73                         | 0.49 $\pm$ 0.72                         |
| 516 Amherstia   | X   | Sq        | 0.16   | 73.10     | 7.49       | 2.6788    | 0.2737 | 12.9                | 3.46 $\pm$ 0.55                        | 1.95 $\pm$ 0.86                         | 1.04 $\pm$ 0.87                         | 1.51 $\pm$ 0.73                         |
| 558 Carmen      | Xk  | -         | 0.12   | 59.31     | 11.38      | 2.9080    | 0.0433 | 8.4                 | 3.47 $\pm$ 0.60                        | -                                       | -                                       | 3.34 $\pm$ 0.78                         |
| 755 Quintilla   | Xk  | Xk        | 0.16   | 36.04     | 4.551      | 3.1729    | 0.1460 | 3.3                 | 3.82 $\pm$ 0.59                        | 2.70 $\pm$ 0.77                         | 0.38 $\pm$ 0.77                         | 2.66 $\pm$ 0.73                         |
| 785 Zwetana     | X   | Xc        | 0.12   | 48.54     | 8.888      | 2.5695    | 0.2099 | 12.7                | 4.03 $\pm$ 0.57                        | 2.60 $\pm$ 0.81                         | 1.80 $\pm$ 0.91                         | 2.78 $\pm$ 0.72                         |
| 849 Ara         | -   | D         | 0.27   | 61.82     | 4.116      | 3.1526    | 0.1961 | 19.5                | 4.50 $\pm$ 0.57                        | 7.96 $\pm$ 0.82                         | 3.78 $\pm$ 0.82                         | 5.48 $\pm$ 0.72                         |
| 860 Ursina      | X   | X         | 0.16   | 29.32     | 9.386      | 2.7947    | 0.1078 | 13.3                | 4.00 $\pm$ 0.57                        | 3.98 $\pm$ 0.82                         | 3.41 $\pm$ 0.80                         | 3.43 $\pm$ 0.71                         |
| 872 Holda       | X   | Xk        | 0.21   | 30.04     | 7.20       | 2.7305    | 0.0801 | 7.3                 | 1.29 $\pm$ 0.56                        | 2.46 $\pm$ 0.76                         | 1.35 $\pm$ 0.72                         | 1.94 $\pm$ 0.71                         |

Table 3: Band center, depth and width for the features detected on the asteroid spectra. The results of the 3  $\mu\text{m}$  band investigation from Rivkin et al. (1995, 2000) are also reported.

| Asteroid       | Band center ( $\mu\text{m}$ ) | Depth (%) | Width ( $\mu\text{m}$ ) | 3 $\mu\text{m}$ band |
|----------------|-------------------------------|-----------|-------------------------|----------------------|
| 16 Psyche      | 0.949 $\pm$ 0.008             | 2.9       | 0.898–1.020             | No                   |
| 16 Psyche      | 0.430 $\pm$ 0.004             | 1.6       | 0.418–0.442             | No                   |
| 22 Kalliope    | 0.903 $\pm$ 0.008             | 2.5       | 0.756–1.017             | Yes                  |
| 22 Kalliope    | 0.434 $\pm$ 0.005             | 1.2       | 0.407–0.456             | Yes                  |
| 55 Pandora     | 0.910 $\pm$ 0.010             | 1.7       | 0.790–0.970             | Yes                  |
| 69 Hesperia    | 0.951 $\pm$ 0.009             | 2.6       | 0.830–1.080             | –                    |
| 69 Hesperia    | 0.430 $\pm$ 0.004             | 1.5       | 0.417–0.443             | –                    |
| 110 Lydia      | 0.942 $\pm$ 0.008             | 2.0       | 0.857–1.033             | Yes                  |
| 125 Liberatrix | –                             | –         | –                       | No                   |
| 129 Antigone   | 1.028 $\pm$ 0.010             | 1.5       | 0.929–1.136             | Yes                  |
| 132 Aethra     | 0.498 $\pm$ 0.004             | 2.0       | 0.456–0.537             | –                    |
| 135 Hertha     | 0.905 $\pm$ 0.008             | 1.9       | 0.771–1.042             | Yes                  |
| 135 Hertha     | 0.515 $\pm$ 0.005             | 1.2       | 0.497–0.531             | Yes                  |
| 161 Athor      | –                             | –         | –                       | No                   |
| 201 Penelope   | –                             | –         | –                       | Yes                  |
| 216 Kleopatra  | 0.969 $\pm$ 0.008             | 3.2       | 0.815–1.104             | No                   |
| 216 Kleopatra  | 0.429 $\pm$ 0.004             | 3.2       | 0.411–0.446             | No                   |
| 250 Bettina    | 0.885 $\pm$ 0.010             | 2.0       | 0.819–0.972             | –                    |
| 338 Budrosa    | 0.876 $\pm$ 0.010             | 2.1       | 0.766–0.981             | –                    |
| 338 Budrosa    | 0.425 $\pm$ 0.004             | 4.2       | 0.407–0.446             | –                    |
| 347 Pariana    | 0.871 $\pm$ 0.008             | 2.4       | 0.780–0.950             | –                    |
| 369 Aeria      | 0.884 $\pm$ 0.008             | 1.9       | 0.772–0.987             | No?                  |
| 498 Tokio      | 0.430 $\pm$ 0.005             | 1.6       | 0.413–0.449             | –                    |
| 498 Tokio      | 1.159 $\pm$ 0.008             | 2.5       | 0.905–1.384             | –                    |
| 516 Amherstia  | 0.965 $\pm$ 0.008             | 6.8       | 0.750–1.440             | –                    |
| 516 Amherstia  | 1.949 $\pm$ 0.010             | 6.1       | 1.702–2.193             | –                    |
| 755 Quintilla  | 0.904 $\pm$ 0.010             | 4.9       | 0.760–1.010             | –                    |
| 755 Quintilla  | 1.864 $\pm$ 0.010             | 3.7       | 1.699–2.062             | –                    |
| 755 Quintilia  | 1.610 $\pm$ 0.008             | 1.9       | 1.535–1.717             | –                    |
| 755 Quintilia  | 1.369 $\pm$ 0.010             | 3.0       | 1.237–1.507             | –                    |
| 785 Zwetana    | –                             | –         | –                       | No                   |
| 872 Holda      | 0.965 $\pm$ 0.020             | 2.8       | 0.866–1.212             | –                    |

Table 4: Summary of the features observed on the asteroids spectra and possible mineralogical interpretation. The Bus-DeMeo (BD) taxonomy is also reported. CFT=crystal field transitions.

| band ( $\mu\text{m}$ ) | asteroids   | BD tax. | suggested mineralogical interpretation                   |
|------------------------|---|---------|--|
| 0.43                   | 16, 22, 69, 216, 338  | Xk      | chlorites and Mg-rich serpentines or pigeonite or augite |
| 0.43                   | 498   | Xc      | iron sulfate jarosite                                    |
| 0.49                   | 132   | -       | sulfides such as oldhamite and/or troilite               |
| 0.51                   | 135   | Xk      | Fe <sup>2+</sup> spin-forbidden CFT in pyroxene          |
| 0.90                   | 16, 22, 55, 69, 110, 135, 216, 250, 338, 347, 369, 755, 872 | Xk      | low-Fe, low-Ca orthopyroxene minerals                    |
| 0.93-1.14              | 129   | Xc      | antigorite?  |
| 0.9-1.3                | 498   | Xc      | unknown  |
| 1.37                   | 755   | Xk      | unknown  |
| 1.61                   | 755   | Xk      | unknown  |
| 1.86                   | 755   | Xk      | iron bearing pyroxene                                    |
| 0.96 and 2             | 516   | Sq      | olivine and pyroxene                                     |

Table 5: The best matches between the 24 asteroid sample observed in the visible and near infrared range and meteorites from the RELAB database.  $\chi^2$  values noted with an asterisk indicate asteroids for which the best RELAB fit matches only the slope and albedo but not the  $0.9 \mu\text{m}$  feature.

| Asteroid        | Albedo | RELAB file    | Met. name         | Met. Class   | Met. Albedo | Grain Size ( $\mu\text{m}$ ) | $\chi^2$ value |
|-----------------|--------|---------------|-------------------|--------------|-------------|------------------------------|----------------|
| 16 Psyche       | 0.12   | eac/sc/s1sc99 | MET101A           | IM           | 0.13        | particulate                  | 6.46667e-04*   |
| 22 Kalliope     | 0.14   | txh/mb/c1mb46 | Landes            | IM           | 0.16        | slab                         | 1.84672e-03    |
| 55 Pandora      | 0.30   | txh/mb/cmmb43 | Esquel            | Pall         | 0.29        | sanded slab                  | 4.15916e-03    |
| 69 Hesperia     | 0.14   | eac/sc/lasc99 | MET101A           | IM           | 0.12        | particulate                  | 8.74344e-04*   |
| 97 Klotho       | 0.23   | mjg/mr/cgp017 | Babb's Mill       | IM           | 0.24        | <300                         | 5.14856e-04    |
| 110 Lydia       | 0.18   | txh/mb/ckmb43 | Esquel            | Pall         | 0.14        | <63                          | 4.52068e-04*   |
| 129 Antigone    | 0.16   | eac/sc/c1sc14 | AWA101            | Iron-Nickel  | 0.11        | 45-90                        | 3.05211e-03    |
| 135 Hertha      | 0.14   | txh/mb/c1mb46 | Landes            | IM           | 0.17        | slab                         | 8.47345e-04    |
| 161 Athor       | 0.20   | mjg/mr/mgn021 | Pillistfer        | EC           | 0.17        | <300                         | 1.46184e-03    |
| 216 Kleopatra   | 0.12   | txh/mb/cfmb47 | DRP78007          | IM           | 0.11        | <25                          | 1.70951e-03    |
| 224 Oceana      | 0.17   | txh/mb/c1mb46 | Landes            | IM           | 0.16        | slab                         | 1.26472e-03    |
| 250 Bettina     | 0.26   | txh/mb/r4mb39 | Y-8451,20         | Pall         | 0.25        | -                            | 1.18340e-03*   |
| 325 Heidelberga | 0.11   | cmp/mi/c1mi08 | Brown (filings)   | IM           | 0.15        | filings                      | 7.68864e-04    |
| 338 Budrosa     | 0.18   | eac/sc/lasc99 | MET101A           | IM           | 0.13        | particulate                  | 1.31101e-03    |
| 347 Pariana     | 0.18   | txh/mb/c1mb46 | Landes            | IM           | 0.17        | slab                         | 9.04683e-04    |
| 369 Aeria       | 0.19   | eac/sc/c1sc99 | MET101A           | IM           | 0.13        | particulate                  | 1.98982e-03*   |
| 441 Bathilde    | 0.14   | atb/ma/c1ma47 | -                 | Laser Irr Ol | 0.12        | >125                         | 2.18014e-03    |
| 498 Tokio       | 0.07   | txh/mb/ncmb59 | Vigarano          | CV           | 0.08        | <100                         | 1.27790e-03    |
| 516 Amherstia   | 0.16   | atb/ma/c1ma53 | Tsarev            | OC*          | 0.14        | >300                         | 5.49437e-04    |
| 755 Quintilla   | 0.16   | txh/mb/cfmb47 | DRP78007          | IM           | 0.12        | <25                          | 1.15605e-02*   |
| 785 Zwetana     | 0.12   | txh/mb/ckmb43 | Esquel            | Pall         | 0.14        | <63                          | 8.76718e-04    |
| 849 Ara         | 0.27   | tjm/tb/c1tb56 | Metal in ALH84019 | Iron-Nickel  | 0.22        | thin section                 | 4.08895e-03    |
| 860 Ursina      | 0.17   | eac/sc/c1sc99 | MET101A           | IM           | 0.13        | particulate                  | 6.02053e-04    |
| 872 Holda       | 0.22   | txh/mb/c1mb46 | Landes            | IM           | 0.16        | slab                         | 2.03065e-03*   |

Table 6: Significant Spearman Correlations (the most significant ones are in bold).

|   | $\rho$           | $P_r$             | $n$       |
|---|------------------|-------------------|-----------|
| <b><math>S_{cont}</math> vs <math>a</math> (all)</b>    | <b>0.638498</b>  | <b>0.00104248</b> | <b>23</b> |
| $S_{cont}$ vs $a$ (with the $0.9\mu\text{m}$ band)      | 0.646493         | 0.0169538         | 13        |
| $S_{cont}$ vs $a$ (without the $0.9\mu\text{m}$ band)   | 0.430303         | 0.214492          | 10        |
| $S_{VIS}$ vs $a$ (all)                                  | 0.311615         | 0.0998569         | 29        |
| $S_{VIS}$ vs $a$ (with the $0.9\mu\text{m}$ band)       | 0.148352         | 0.628610          | 13        |
| $S_{VIS}$ vs $a$ (without the $0.9\mu\text{m}$ band)    | 0.426471         | 0.0994991         | 16        |
| <b><math>S_{NIR1}</math> vs <math>a</math> (all)</b>    | <b>0.630435</b>  | <b>0.00126108</b> | <b>23</b> |
| $S_{NIR1}$ vs $a$ (with the $0.9\mu\text{m}$ band)      | 0.571429         | 0.0413423         | 13        |
| $S_{NIR1}$ vs $a$ (without the $0.9\mu\text{m}$ band)   | 0.642857         | 0.0855589         | 10        |
| $S_{NIR2}$ vs $a$ (all)                                 | 0.331604         | 0.122167          | 23        |
| $S_{NIR2}$ vs $a$ (with the $0.9\mu\text{m}$ band)      | 0.0494505        | 0.872543          | 13        |
| $S_{NIR2}$ vs $a$ (without the $0.9\mu\text{m}$ band)   | 0.498483         | 0.142518          | 10        |
| <b><math>S_{cont}</math> vs <math>rot</math> (all)</b>  | <b>-0.418088</b> | <b>0.0471146</b>  | <b>23</b> |
| $S_{cont}$ vs $rot$ (with the $0.9\mu\text{m}$ band)    | -0.162311        | 0.596258          | 13        |
| $S_{cont}$ vs $rot$ (without the $0.9\mu\text{m}$ band) | -0.406061        | 0.244282          | 10        |
| <b><math>S_{NIR1}</math> vs <math>rot</math> (all)</b>  | <b>-0.482213</b> | <b>0.0197941</b>  | <b>23</b> |
| $S_{NIR1}$ vs $rot$ (with the $0.9\mu\text{m}$ band)    | -0.0274725       | 0.929013          | 13        |
| $S_{NIR1}$ vs $rot$ (without the $0.9\mu\text{m}$ band) | -0.466667        | 0.173939          | 10        |
| <b><math>S_{NIR2}</math> vs <math>rot</math> (all)</b>  | <b>-0.516926</b> | <b>0.0115455</b>  | <b>23</b> |
| $S_{NIR2}$ vs $rot$ (with the $0.9\mu\text{m}$ band)    | -0.478022        | 0.0984901         | 13        |
| $S_{NIR2}$ vs $rot$ (without the $0.9\mu\text{m}$ band) | -0.547115        | 0.101678          | 10        |
| <b><math>S_{VIS}</math> vs <math>alb</math> (all)</b>   | <b>-0.486513</b> | <b>0.00744684</b> | <b>29</b> |
| $S_{VIS}$ vs $alb$ (with the $0.9\mu\text{m}$ band)     | -0.329670        | 0.271335          | 13        |
| $S_{VIS}$ vs $alb$ (without the $0.9\mu\text{m}$ band)  | -0.635294        | 0.00818205        | 16        |

## Figure captions

Fig. 1 - Visible spectra of 6 M-type asteroids. For 125 Liberatrix three spectra were acquired on 2004, November 20: the spectrum labelled A corresponds to UT=20:37, the B to UT=22:01, and the C to UT=23:27.

Fig. 2 - Observed spectra for Tholen M-type asteroids extended into the near-infrared.

Fig. 3 - Observed spectra for Tholen M-type asteroids extended into the near-infrared.

Fig. 4 - Observed spectra for Tholen M-type asteroids extended into the near-infrared.

Fig. 5 - Observed spectra for Tholen M-type asteroids extended into the near-infrared.

Fig. 6 - Spectral matches between the featureless observed asteroids (in black) and meteorites (in red) from the RELAB database (see Table 5 for details on the meteorites samples).

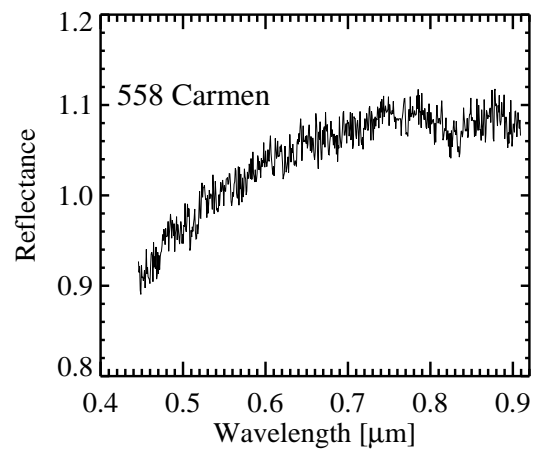
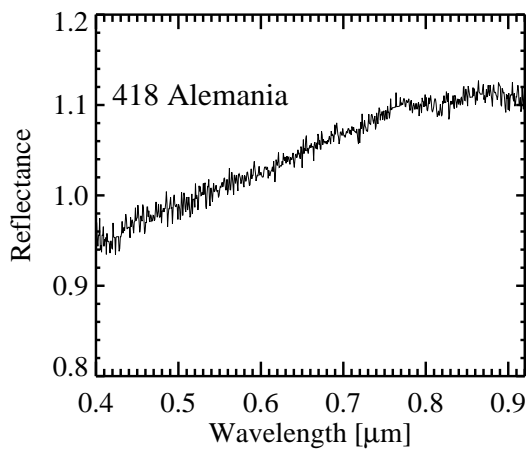
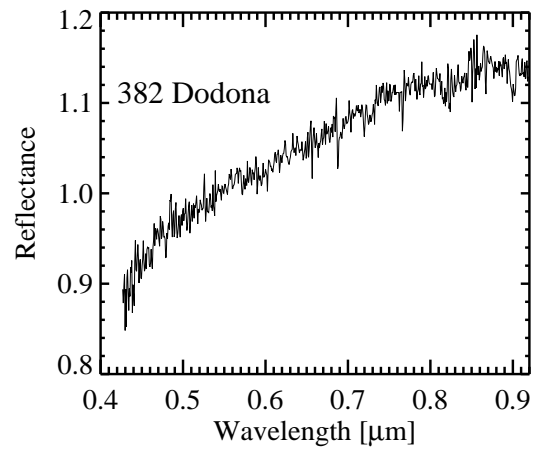
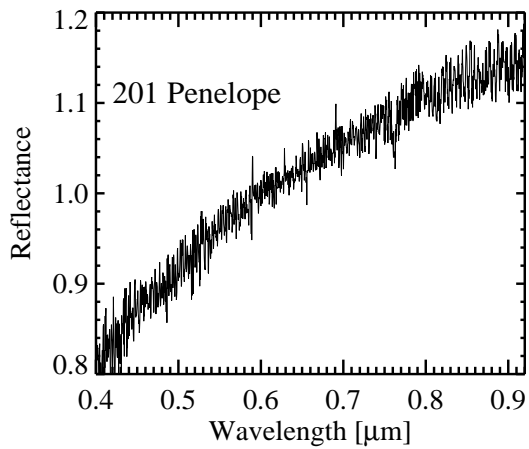
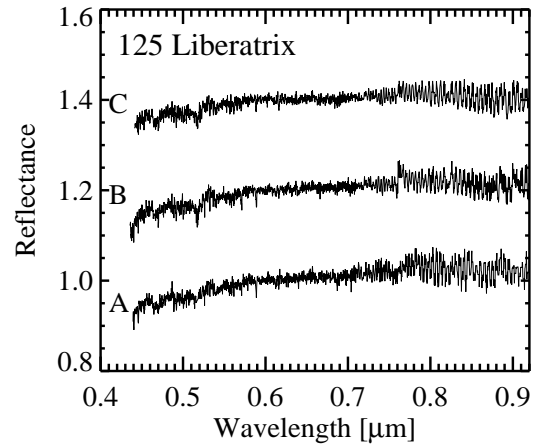
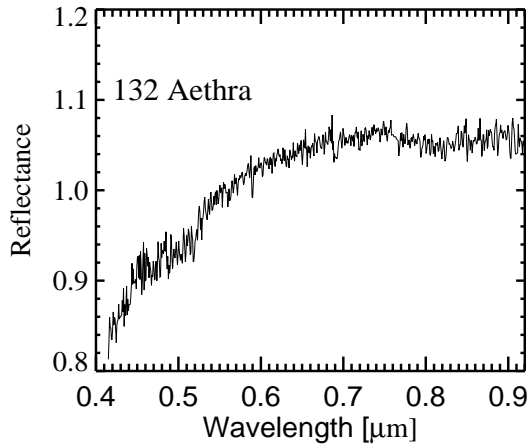
Fig. 7 - Spectral matches between the observed asteroids (in black) showing the  $0.43 \mu\text{m}$  feature and meteorites (in red) from the RELAB database (see Table 5 for details on the meteorites samples). In the Bus-Demeo taxonomy all these asteroids, except 498 Tokio (Xc-type), belong to the Xk-type and show also a band in the  $0.9 \mu\text{m}$  region

Fig. 8 - Spectral matches between the observed asteroids (in black) having absorption features beyond  $0.8 \mu\text{m}$  and meteorites (in red) from the RELAB database (see Table 5 for details on the meteorites samples). All asteroids belong to the Xk-type in the Bus-Demeo taxonomy, except 129 Antigone (Xc-type), and 516 Amherstia (Sq-type).

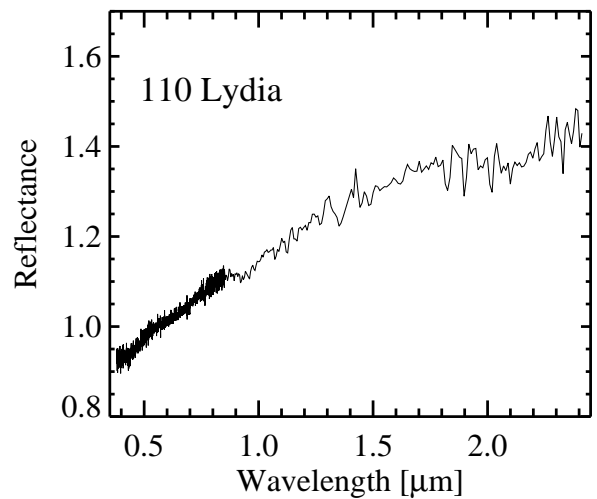
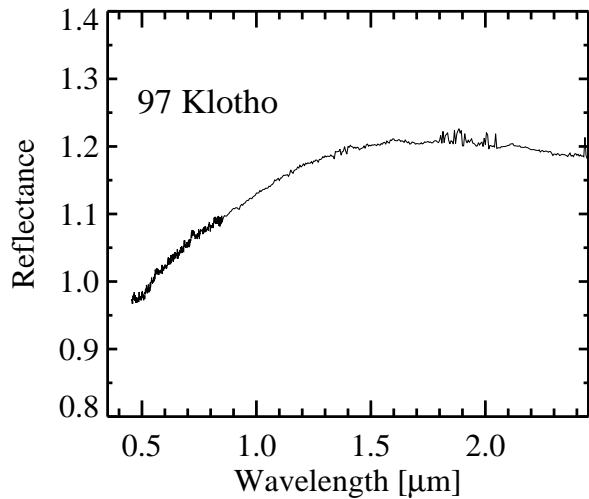
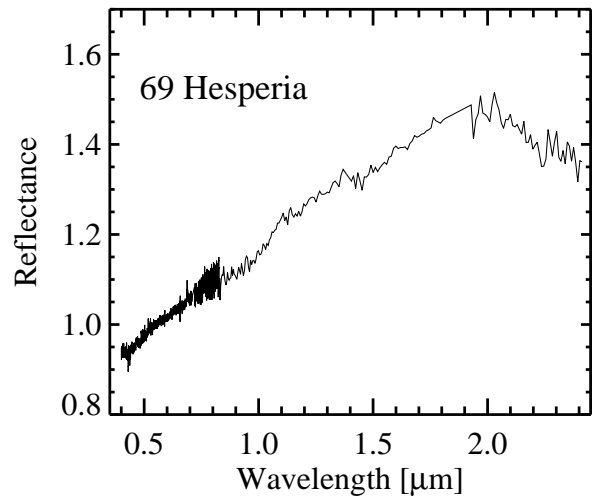
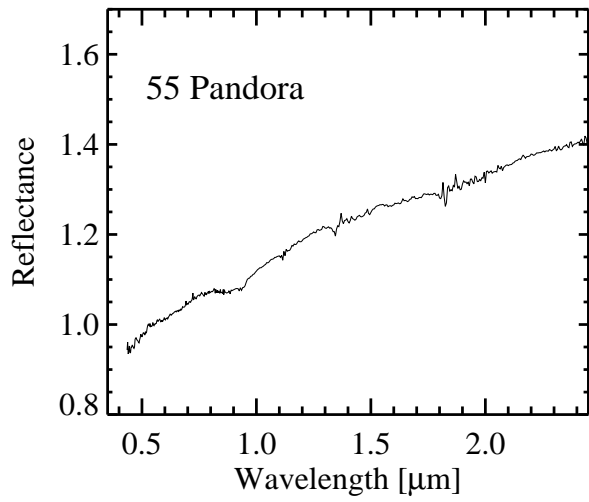
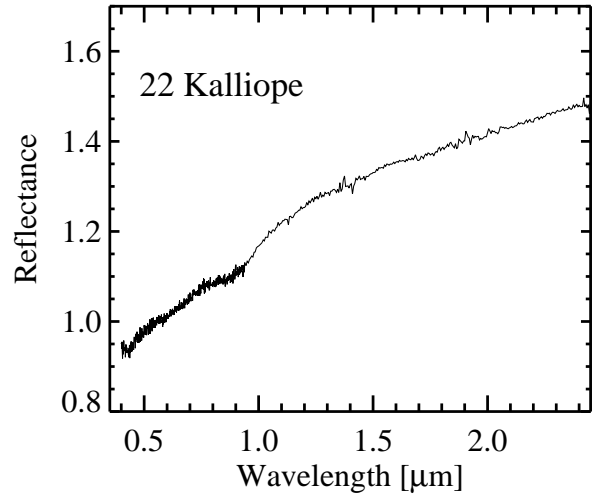
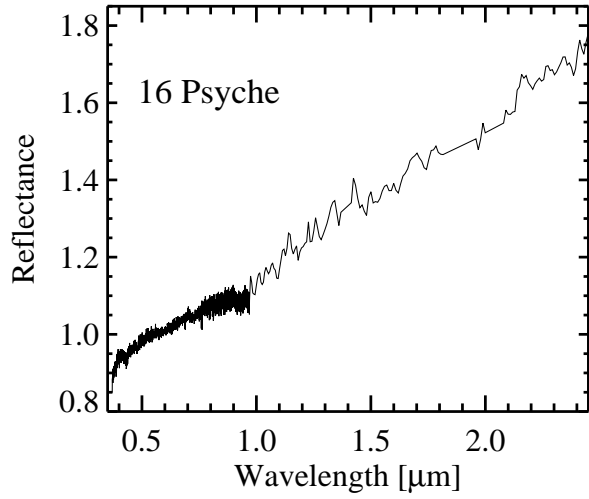
Fig. 9 - Visual and NIR1 slopes versus the semi-major axis, albedo and rotational period for the observed asteroids. Black bullet represent the asteroids showing a band in the  $0.9 \mu\text{m}$  region and belonging to the Xk-type in the Bus-DeMeo taxonomy.

Fig. 10 - Geophysical mixtures proposed to interpret the surface composition of 22 Kalliope: 98% pallasite and 2% goethite (continuous line, mixture albedo = 0.14); 99% pallasite and 1.0% orthopyroxene (dashed line, mixture albedo = 0.14).

## Figures

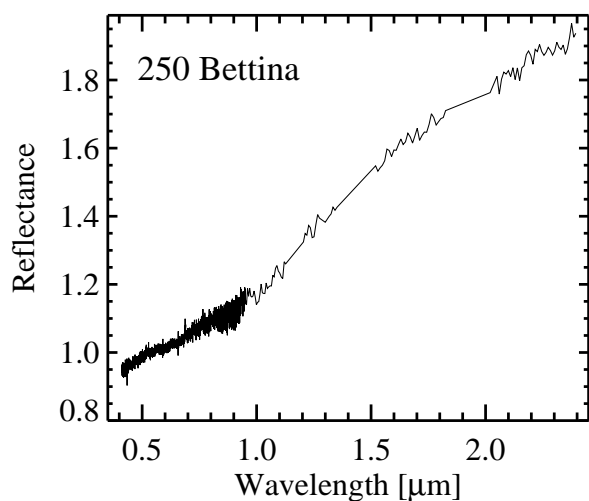
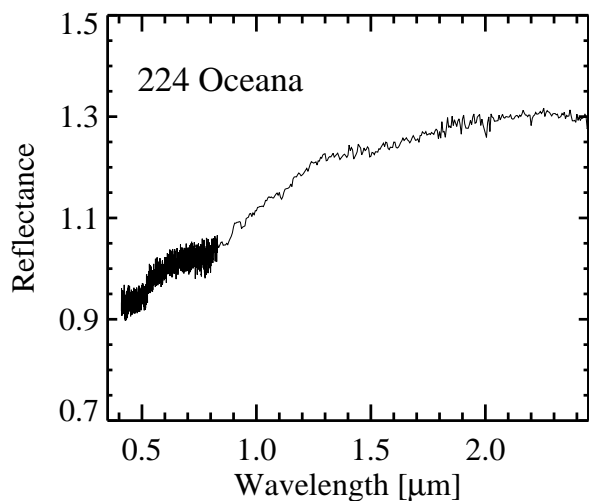
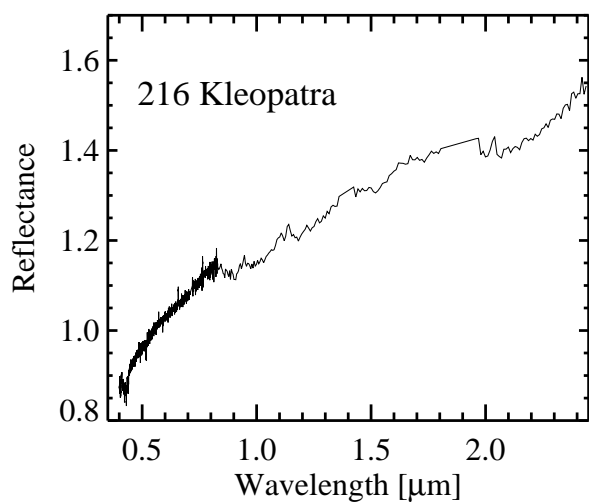
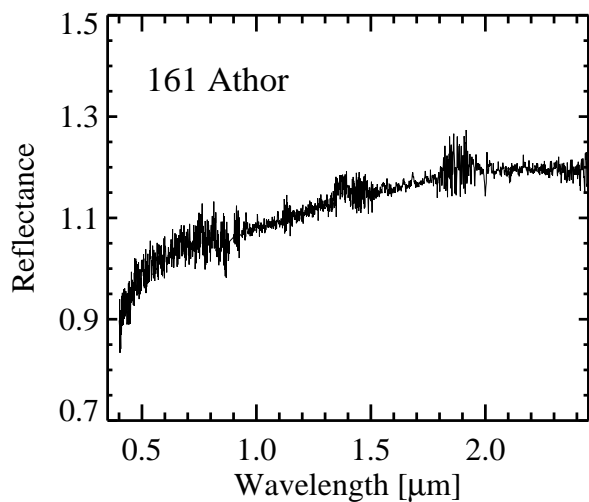
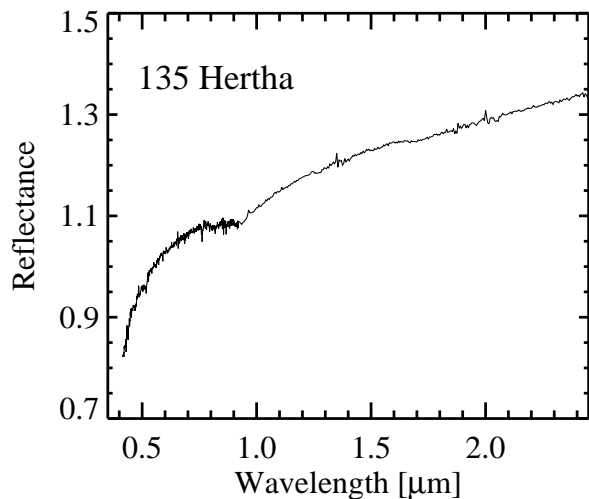
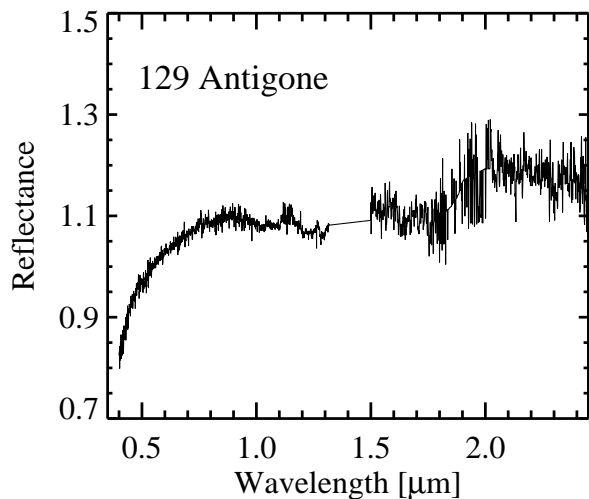


40  
Figure 1:



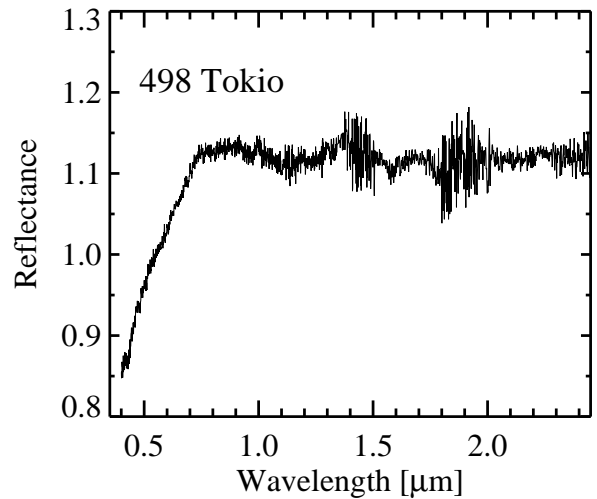
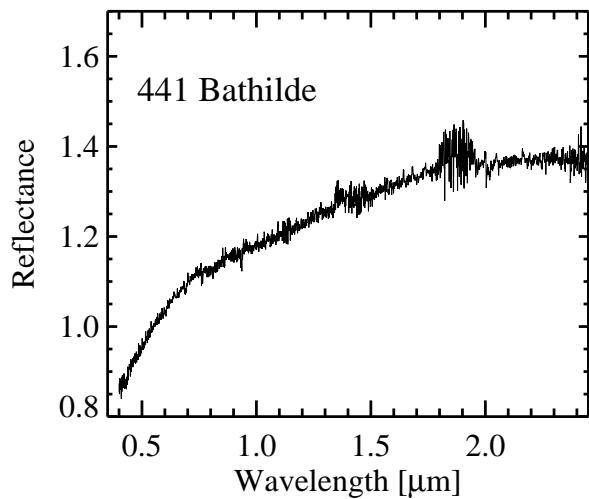
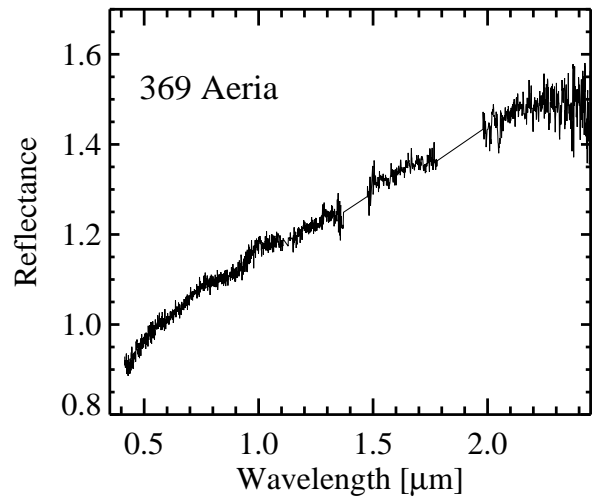
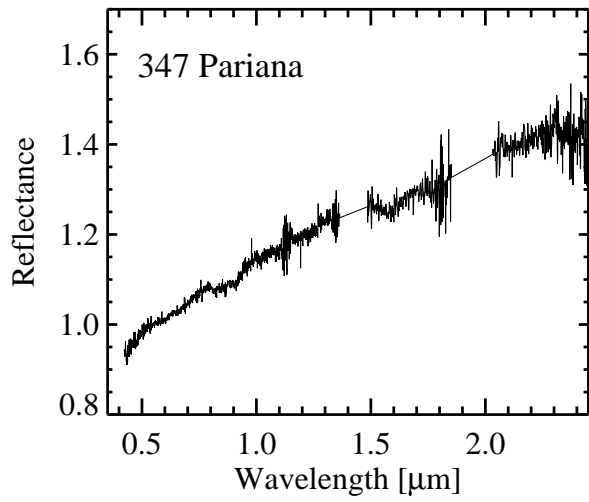
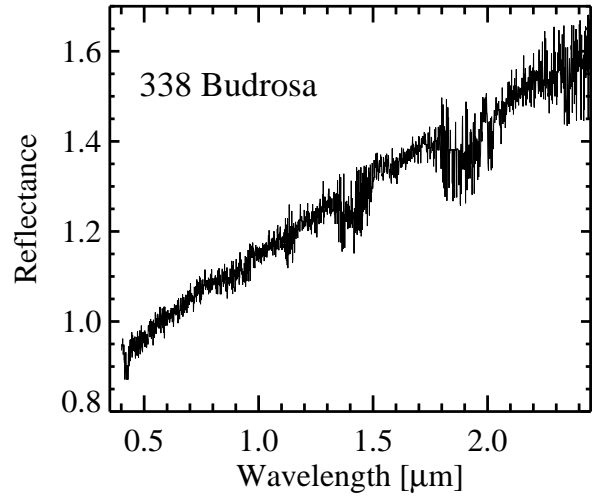
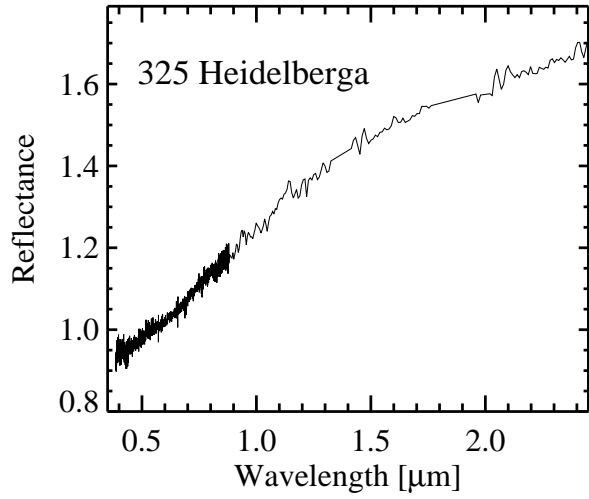
41

Figure 2:



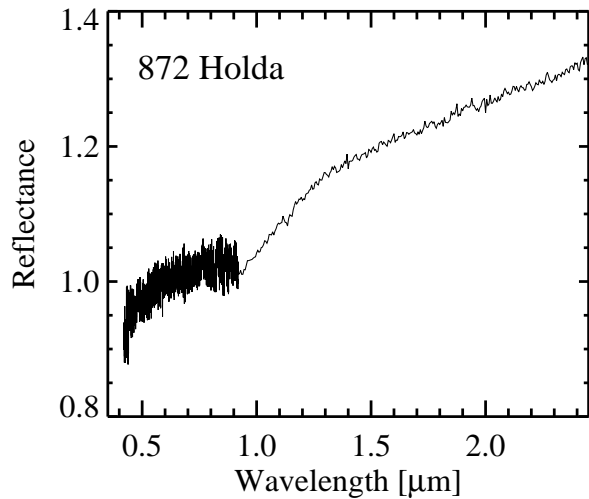
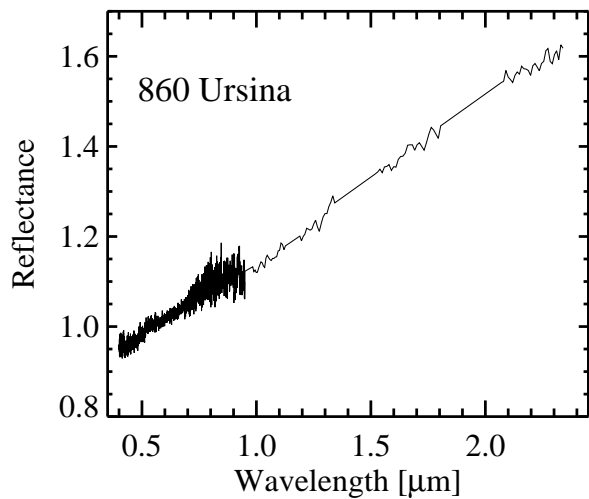
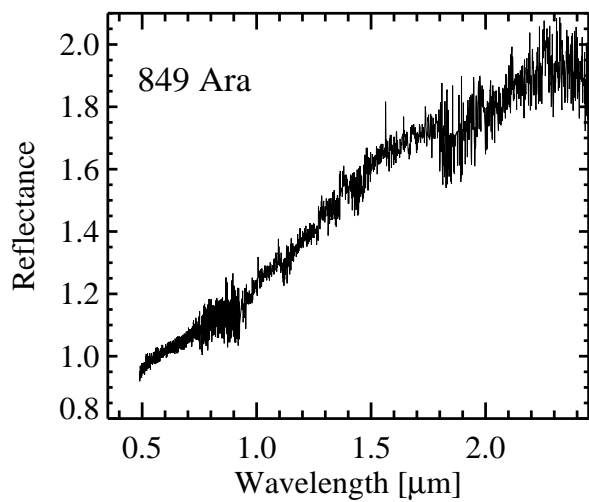
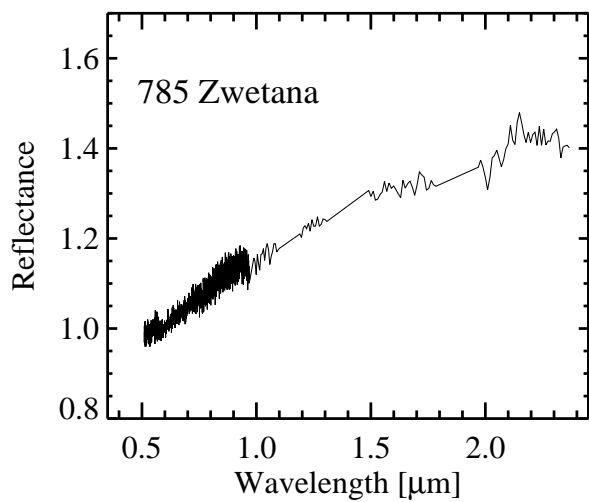
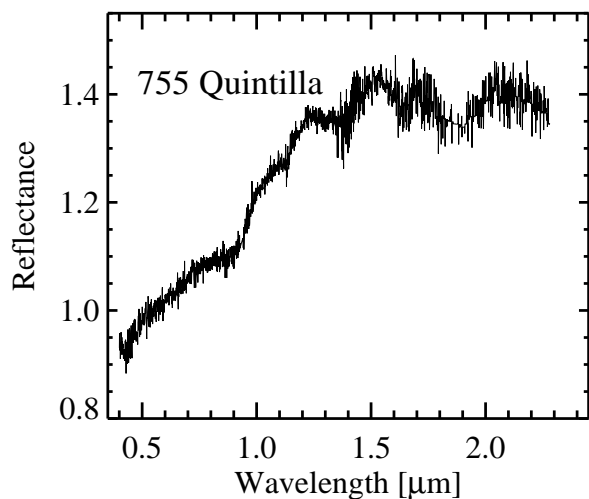
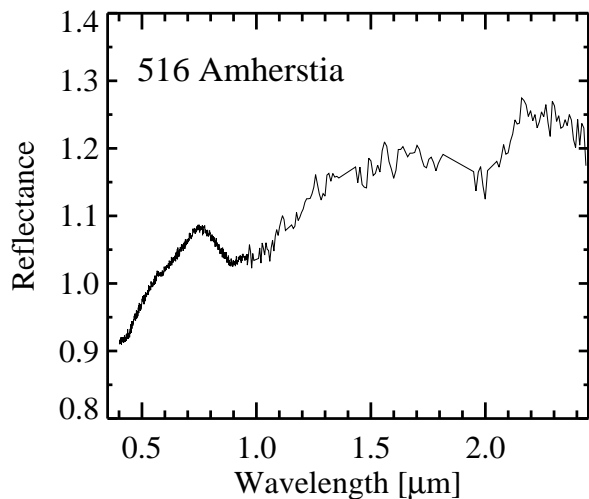
42

Figure 3:



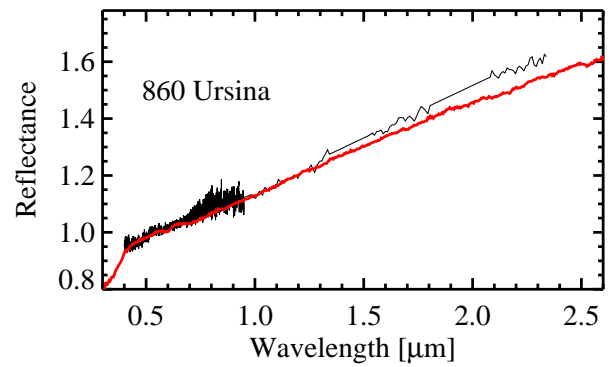
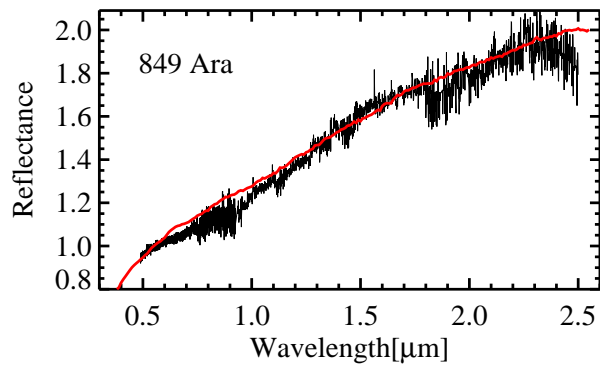
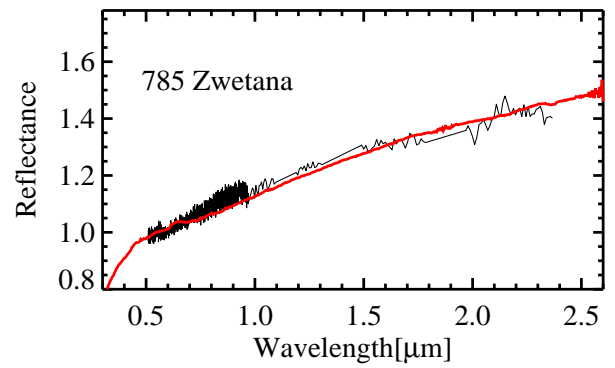
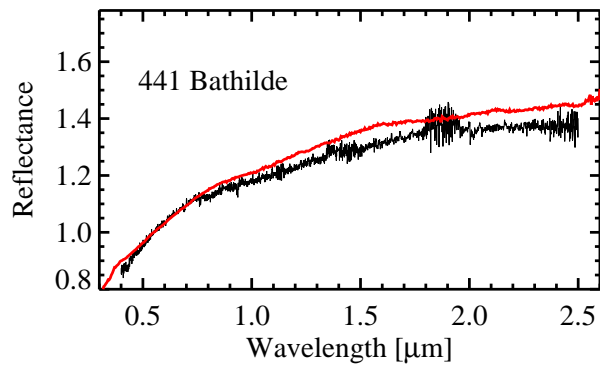
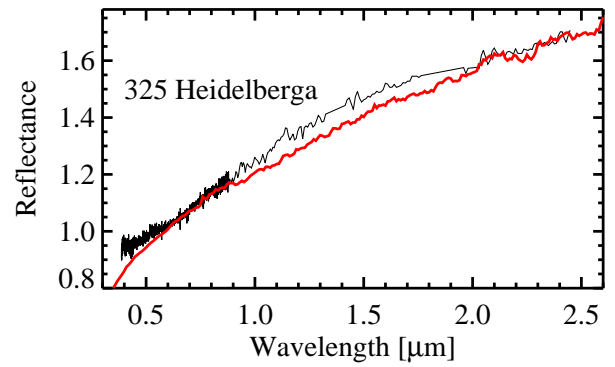
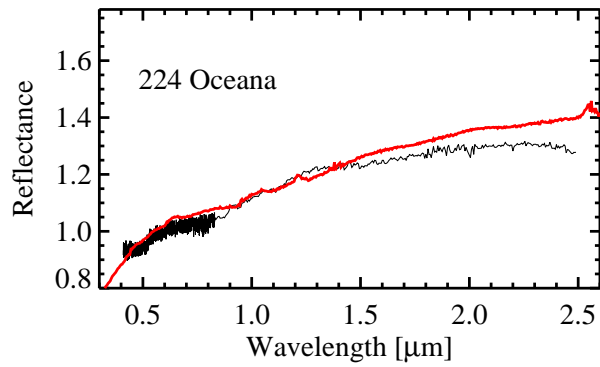
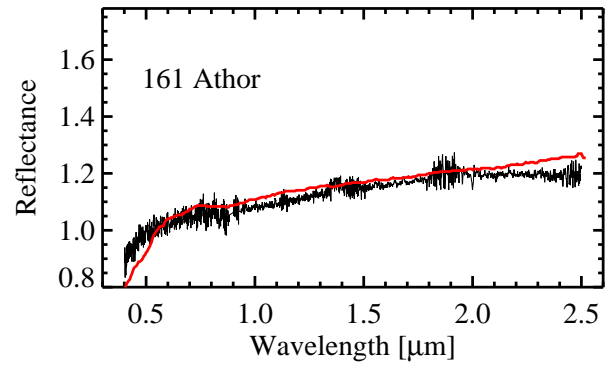
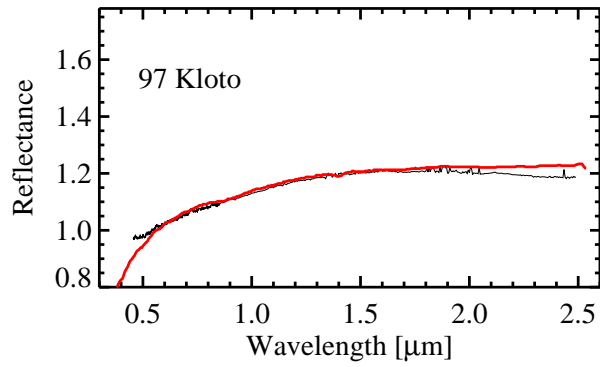
43

Figure 4:



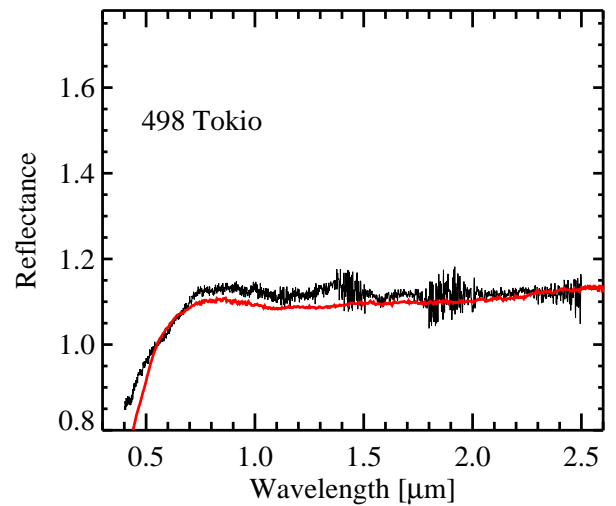
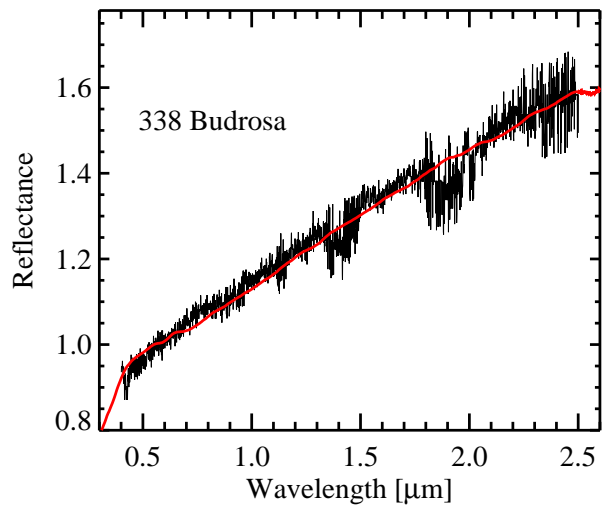
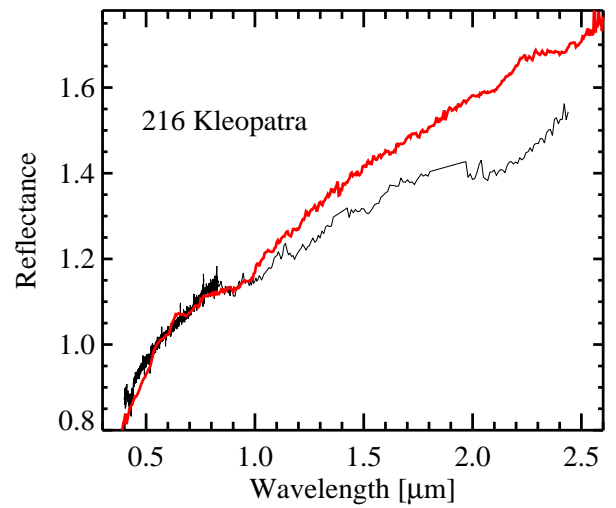
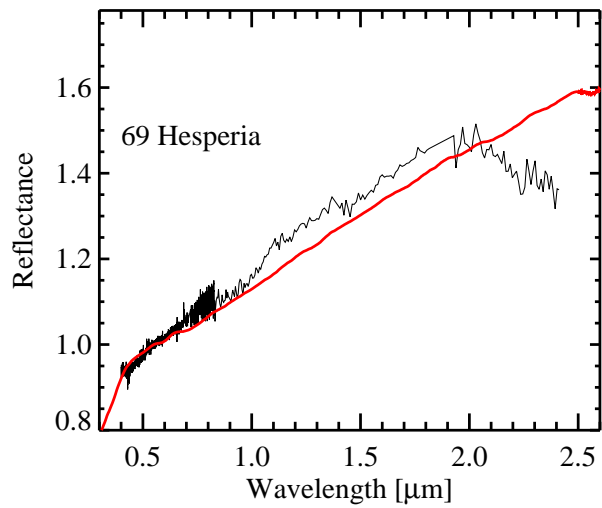
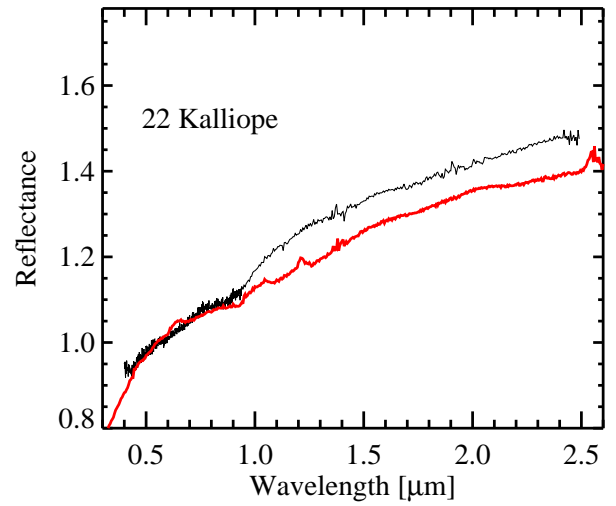
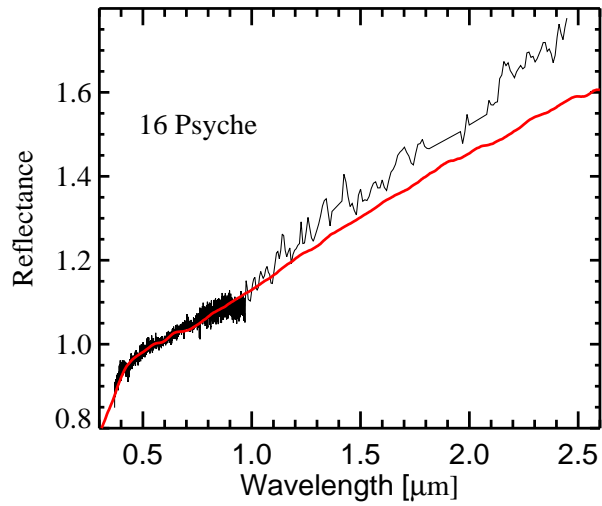
44

Figure 5:



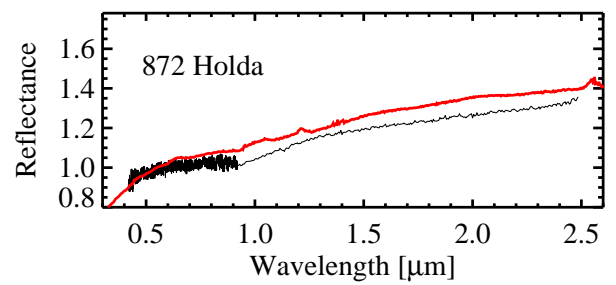
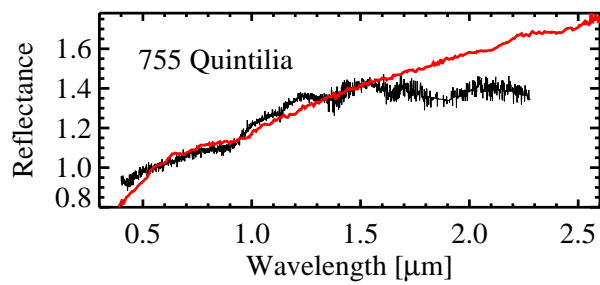
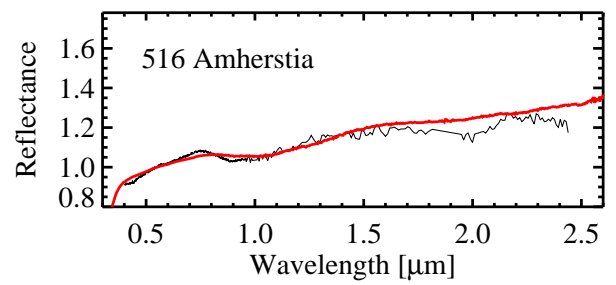
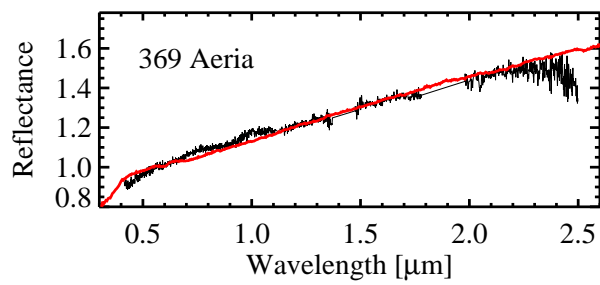
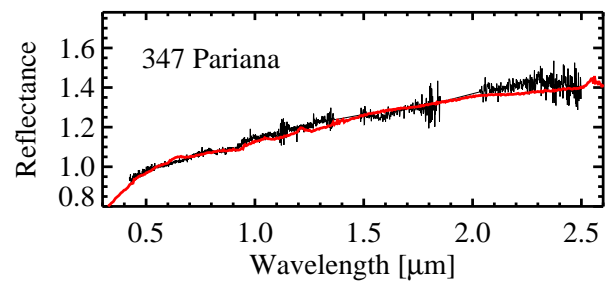
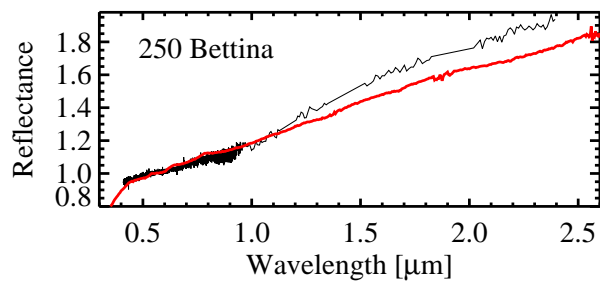
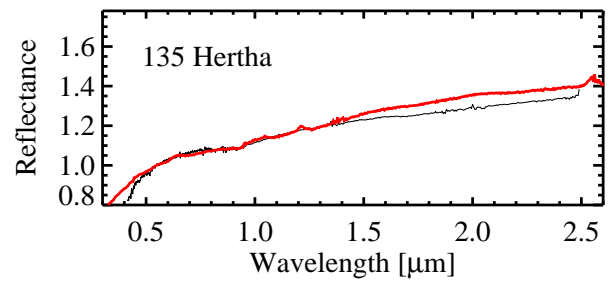
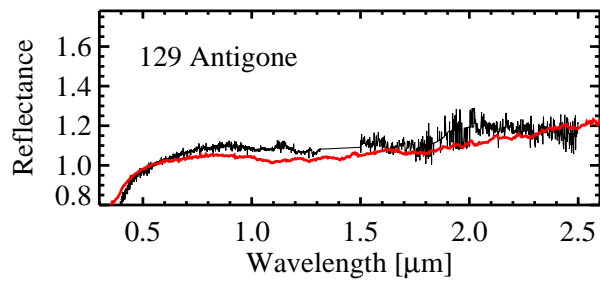
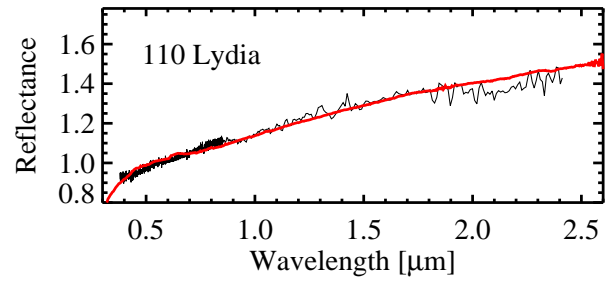
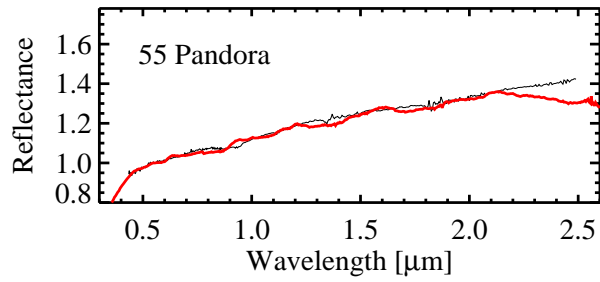
45

Figure 6:



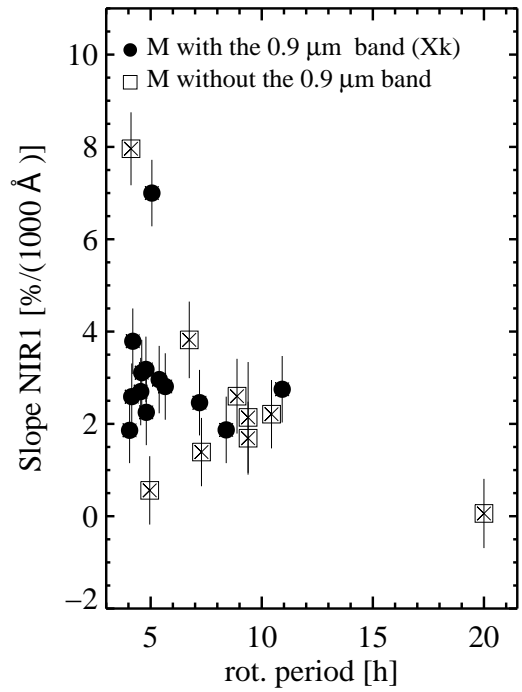
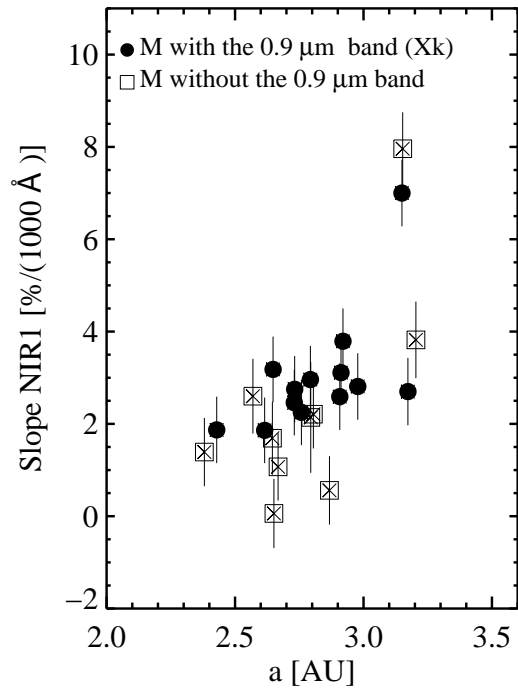
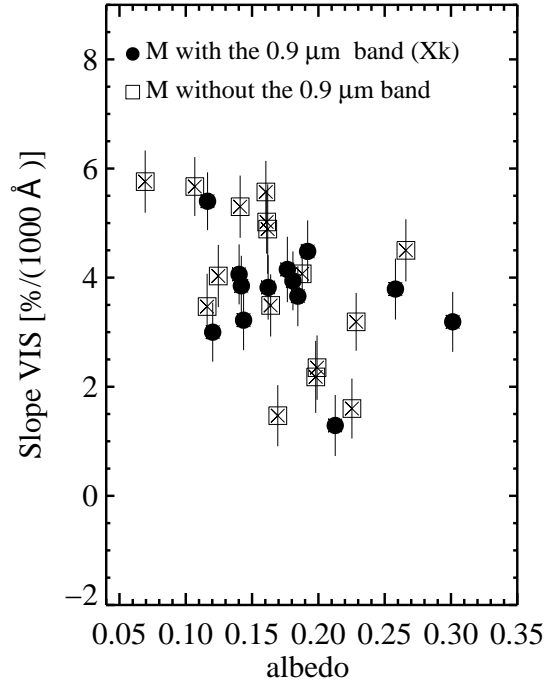
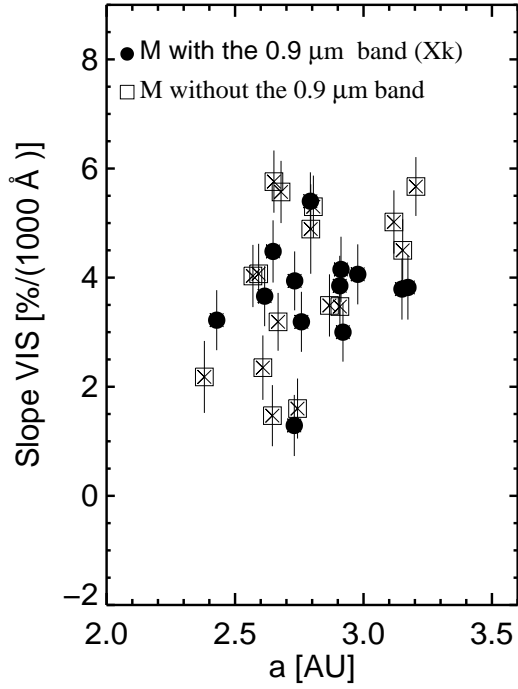
46

Figure 7:



47

Figure 8:



48  
 Figure 9:

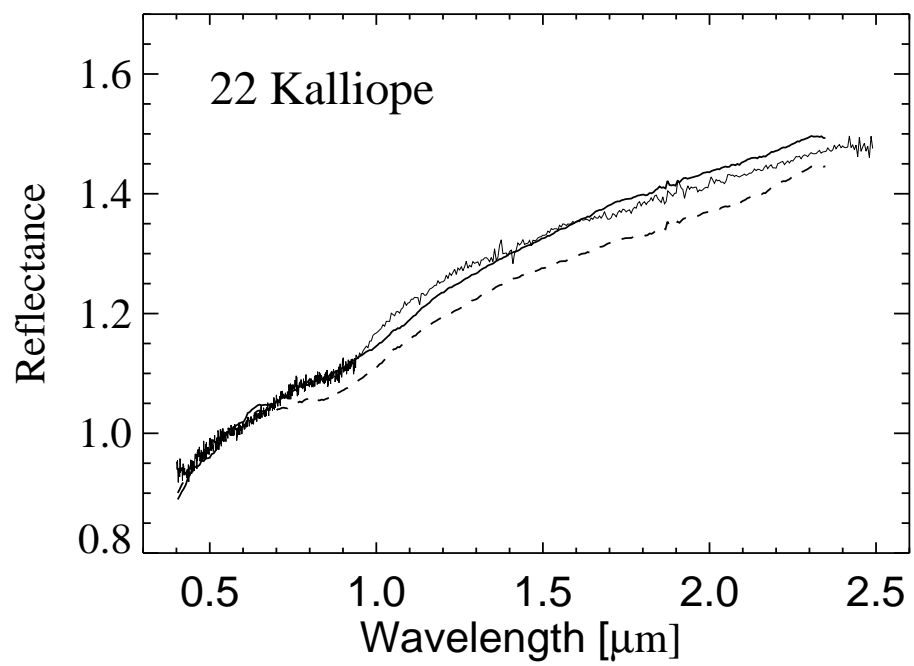


Figure 10: